CHAPTER 6

Ultrafast Nonlinear Optical Signals Viewed from the Molecule's Perspective: Kramers–Heisenberg Transition-Amplitudes versus Susceptibilities

Shaul Mukamel and **Saar Rahav**

Department of Chemistry, University of California, Irvine, CA 92697, USA

Contents

Advances in Atomic, Molecular, and Optical Physics, Volume 59
ISSN 1049-250X, DOI: 10.1016/S1049-250X(10)59006-2

Abstract

Coherent nonlinear optical signals are commonly calculated using a semiclassical approach that assumes a quantum system interacting with classical fields. Compact expressions for the signals are then derived in terms of nonlinear susceptibilities. We present an alternative approach based on a quantum description of both matter and field. The signals are further recast in terms of transition amplitudes, which provide a clearer picture for the underlying molecular processes and may be intuitively represented by closed-time-path-loop diagrams. Unlike the semiclassical approach that treats the signal mode macroscopically using Maxwell's equations, the present formalism allows for a fully microscopic calculation of the entire process. For example, $n+1$ wave mixing appears as a concerted $n+1$ photon event and all $n+1$ field modes (including the signal) are treated on the same footing. Resonant contributions to nonlinear optical signals that carry useful molecule-specific information are recast as the modulus square of transition amplitudes and are clearly separated from the parametric background. Purely dissipative signals that can be measured using a collinear beam geometry and manipulated by pulse shaping techniques are proposed. The approach is demonstrated by applications to the stimulated Raman and the two-photon absorption components of pump–probe, and to coherent anti-Stokes Raman spectroscopy.

1. INTRODUCTION

Nonlinear spectroscopy provides detailed information on molecular structure and dynamical processes through specific electronic or vibrational resonances. Spectroscopic techniques may be broadly classified as frequency- or time-domain type and are conveniently and systematically analyzed order by order in the incoming fields. In the semiclassical (quantum matter coupled to classical fields) description of an $n+1$ wave mixing process, the system is subjected to n incoming pulses that generate an n'th order polarization $P^{(n)}$ (Mukamel, 1995; Scully & Zubairy, 1997; Shen, 2002)

$$P^{(n)}(t) = \int_0^\infty \mathrm{d}t_1 \cdots \int_0^\infty \mathrm{d}t_n S^{(n)}(t_n, \ldots, t_1) E(t - t_n) \cdots E(t - t_n \cdots - t_1). \quad (1)$$

This can be alternatively recast in the frequency domain

$$P^{(n)}(\omega) = \int \mathrm{d}\omega_1 \cdots \int \mathrm{d}\omega_n \chi^{(n)}(-\omega; \omega_1, \ldots, \omega_n) E(\omega_1) \cdots E(\omega_n), \quad (2)$$

where $E(\omega) = \int \mathrm{d}t E(t) \mathrm{e}^{\mathrm{i}\omega t}$. The response functions $S^{(n)}$ or their frequency domain counterparts, the susceptibilities $\chi^{(n)}$, contain all the material information necessary for calculating and analyzing n'th order processes. The signal field is calculated by substituting $P^{(n)}$ as a source in Maxwell's equations.

The homodyne detected signal is quadratic in the polarization

$$S^{(n)}_{\mathrm{HOM}} \sim \int \left| P^{(n)}(t) \right|^2 \mathrm{d}t, \quad (3)$$

while heterodyne signals (Figure 1) depend linearly on the polarization and provide both its amplitude and its phase (Mukamel, 1995)

$$S^{(n)}_{\mathrm{HET}} \sim \int \Im E(t) P^{(n)}(t) \mathrm{d}t. \quad (4)$$

[For the precise expression see Equation (21).]

One problem with the molecular-level interpretation of optical signals is that the polarization (like any other quantum observable) is determined by interactions occurring on both the bra and the ket of the matrix elements of the dipole operator μ

$$P^{(n)}(t) = \sum_{m=0}^{n} \langle \psi^{(m)}(t) | \hat{\mu} | \psi^{(n-m)}(t) \rangle. \quad (5)$$

Here $\left| \psi^{(n)}(t) \right\rangle$ is the wave function calculated to n'th order in the field–matter interaction $\mathcal{H}_{\mathrm{int}}$ [Equation (13)]. The susceptibilities depend on various *Liouville space pathways* which count the various orders in Equation (5) as well as the relative time ordering of the interactions. Different pathways interfere, and this interference complicates the simple intuitive interpretation of signals.

In an alternative approach, some optical signals are traditionally interpreted in terms of *transition amplitudes* rather than susceptibilities. The description of four-wave mixing signal from an ensemble of two-level atoms in terms of transition amplitudes was discussed by Dubetsky and Berman (1993). A notable example is the Kramers– Heisenberg formula for spontaneous light emission (Cohen-Tannoudji et al., 1997) where a photon ω_1 is absorbed and ω_2 is emitted

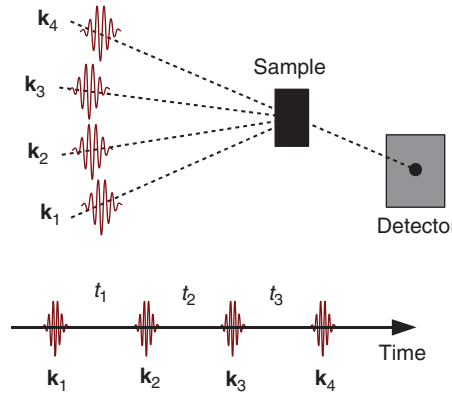

Figure 1 Schematic depiction of a heterodyne detected four-wave mixing process. The signal is generated in the direction $\mathbf{k}_4 = \pm\mathbf{k}_1 \pm \mathbf{k}_2 \pm \mathbf{k}_3$. Here the incoming $\mathbf{k}_4$ beam passes through the sample and stimulates the signal. In ordinary heterodyne detection the beam mixes only with the signal and does not pass through the sample. The two configurations yield identical signals to the first order in the $\mathbf{k}_4$ beam amplitude

$$S(\omega_1, \omega_2) = \sum_{a,c} P(a)|\mathcal{E}_1|^2 \left|\tilde{T}_{ca}\right|^2 \delta(\omega_1 - \omega_2 - \omega_{ca}). \tag{6}$$

Here

$$\tilde{T}_{ca} = \sum_b \frac{\mu_{cb}\mu_{ba}}{\omega_1 - \omega_{ba} + \mathrm{i}\eta}, \tag{7}$$

is the transition amplitude and $P(a)$ the equilibrium population of state a. [Two-photon absorption is also given by Equation (6), by replacing $\omega_1 - \omega_2$ with $\omega_1 + \omega_2$.] There is no ambiguity as to what is going on in the molecule in this formulation. The signal is given by the modulus square of a transition amplitude $\tilde{T}_{ca}$ from the initial ($|a\rangle$) to the final ($|c\rangle$) state. That transition amplitude is in turn given by the sum over all possible quantum pathways which may contain interferences. The interference of single- and two-photon pathways in photoelectron detection (Figure 2) was pointed out by Glauber (2007). In this case the transition amplitude has the form

$$\tilde{T}_{ca} = \mu_{ca}E(2\omega) + \frac{\mu_{cb}\mu_{ba}}{\omega - \omega_{ba} + \mathrm{i}\eta}E^2(\omega). \tag{8}$$

This interference may be controlled by varying the relative phase of the two fields $E(\omega)$ and $E(2\omega)$. A simpler interference between one and two photon processes was used to control the photocurrents in semiconductors by varying the relative phase of the two beams (Haché et al., 1997).

In this review we address the following question: under what conditions is it possible to represent heterodyne detected nonlinear optical

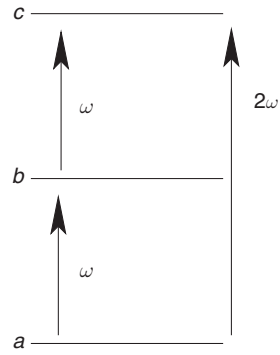

Figure 2 The transition pathways of Equation (8). A direct transition where a single 2ω photon is absorbed interferes with the absorption of two ω photon

signals in terms of transition amplitudes rather than susceptibilities? Apart from the obvious advantage for the interpretation, amplitudes are simpler to calculate, since they are lower order and contain fewer terms than susceptibilities. The results presented here have been developed in a series of articles (Marx et al., 2008; Rahav & Mukamel, 2010; Rahav et al., 2009; Roslyak et al., 2009). Here we provide an overview and discuss possible generalizations.

By using a quantum description of the field we show that examination of the relevant processes from the viewpoint of the material naturally leads to a description in terms of transition amplitudes rather than susceptibilities. Once the optical signals have been recast in terms of these transition amplitudes, the material processes involved become evident. We further show that nonlinear signals generally contain two types of contributions: resonant *dissipative* processes where the matter participates actively and changes its state at the end, and *parametric* processes where the matter only serves as a passive "catalyst" for exchange of energy among field modes and it returns to its initial state at the end of the process. Only the former, which are most interesting for spectroscopic applications, can be generally recast in a generalized Kramers–Heisenberg form, whereas the latter merely provide an off-resonant background. Intuitive closed-time-path-loop (CTPL) diagrams will be introduced and used to dissect the signal into the two components. We further discuss signals that eliminate the parametric process and solely provide the desired resonant contributions. These ideas will be illustrated by applications to pump–probe spectroscopy and to coherent anti-Stokes Raman spectroscopy (CARS).

The structure of this review is as follows. Sections 2–4 contain the necessary background material for the fully quantum calculation and

analysis of optical signals. In Section 2 we present a quantum field approach for the calculation of heterodyne detected signals. Here all $n+1$ active field modes are considered on the same footing. In Section 3 we examine optical processes from the viewpoint of the material degrees of freedom and introduce the transition amplitudes which represent the material processes. CTPL diagrams provide a convenient bookkeeping tool for nonlinear optical signals. These are introduced in Section 4.

In Sections 5–8 we calculate the optical signals and dissect them into various contributions from material processes. Pump–probe (two-photon absorption and stimulated Raman) signals are presented in Sections 5 and 6, whereas CARS signals are described in Sections 7 and 8. Using the results of Section 8 we show in Section 9 that the resonant part of the CARS signal can be interpreted as originating from double-slit interference. In Section 10 we show that the purely dissipative signals, defined in Section 3.1, can be used to distinguish between different resonant transitions in matter. We conclude in Section 11 with some remarks on the generality of the present approach.

2. QUANTUM-FIELD DESCRIPTION OF HETERODYNE SIGNALS

Traditionally, nonlinear optical signals are calculated in a semiclassical framework whereby a classical field interacts with quantum matter (Mukamel, 1995; Scully & Zubairy, 1997; Shen, 2002). This assigns different roles to the n fields interacting with the system and to the $(n+1)$'th "local oscillator" field used for heterodyne detection. In the following we present a fully quantum description of both matter and field. In this approach, which can describe both spontaneous and stimulated processes, the system is allowed to interact with the "local oscillator," and the signal measures the change of the number of photons in the detected modes. $n+1$ wave mixing naturally appears as a single event involving all $n+1$ field modes which are treated on an equal footing.

A molecule interacting with an optical field is described by the Hamiltonian

$$\hat{H} = \hat{H}_0 + \hat{H}_{\rm F} + \hat{H}_{\rm int}, \tag{9}$$

where $\hat{H}_0$ represents the free molecule, and

$$\hat{H}_{\rm F} = \sum_s \hbar\omega_s \hat{a}_s^\dagger \hat{a}_s, \tag{10}$$

is the Hamiltonian of the field degrees of freedom. The optical electric field operator is

$$\hat{E}(\mathbf{r},t) = \hat{\mathcal{E}}(\mathbf{r},t) + \hat{\mathcal{E}}^\dagger(\mathbf{r},t), \tag{11}$$

with the positive-frequency component

$$\hat{\mathcal{E}}(\mathbf{r},t)=\sum_s\left(\frac{2\pi\hbar\omega_s}{\Omega}\right)^{1/2}\hat{a}_s\,\mathrm{e}^{\mathrm{i}\mathbf{k}_s\cdot\mathbf{r}-\mathrm{i}\omega_s t}. \tag{12}$$

The quantities $\hat{a}_s^\dagger(\hat{a}_s)$ are boson creation (annihilation) operators, Ω is the quantization volume, and cgs units are used.

The molecule–field interaction in the rotating wave approximation (RWA), which neglects off-resonant terms, is given by

$$\hat{H}_{\mathrm{int}}(t)=\hat{\mathcal{E}}(\mathbf{r},t)\hat{V}^\dagger+\hat{\mathcal{E}}^\dagger(\mathbf{r},t)\hat{V}, \tag{13}$$

where $\hat{V}=\Sigma_a\Sigma_{b>a}\mu_{ab}|a\rangle\langle b|$ is the part of the dipole operator describing transitions down in energy.

The entire molecule+field system is represented by the density matrix $\hat{\rho}(t)$. We denote expectation values with respect to this density matrix by $(\cdots)_\rho$. Using perturbation theory these will be expanded in terms of averages $\langle\cdots\rangle$ over the initial non-interacting density matrix at $t\to-\infty$.

In a quantum description of time-domain optical signals where the system interacts with the field only during finite pulses, the signal S is defined as the net change of the photon number between the initial (i) and final (f) states, that is

$$S\equiv\int\mathrm{d}t\frac{\mathrm{d}}{\mathrm{d}t}(\hat{\mathcal{N}})_\rho=\langle\hat{\mathcal{N}}\rangle_{\mathrm{f}}-\langle\hat{\mathcal{N}}\rangle_{\mathrm{i}}, \tag{14}$$

where

$$\hat{\mathcal{N}}\equiv\sum_s\hat{a}_s^\dagger\hat{a}_s, \tag{15}$$

and the sum runs over the detected modes.

Taking the frequency domain (FD) limit should be done with care, since Equation (14) may turn out to be infinite. It is then natural to drop the t integration in the definition of the signal and redefine it as the *rate* of change in the number of photons,

$$S\equiv\frac{\mathrm{d}}{\mathrm{d}t}(\hat{\mathcal{N}})_\rho \tag{16}$$

We will use both definitions of the signal in the following. Equation (16) is adequate for the pump–probe application studied in Section 5. Equation (14) will be used in Section 7 for the CARS signal. The reasons behind this will be discussed in the relevant sections.

The time derivative in Equation (14) or (16) will be calculated using the Heisenberg equations of motion and the Hamiltonian Equation (9)

$$\frac{\mathrm{d}}{\mathrm{d}t}\left(\hat{\mathcal{N}}\right)_\rho \equiv \left\langle \frac{\mathrm{d}}{\mathrm{d}t}\hat{\mathcal{N}}_H \right\rangle = \left\langle \sum_s \frac{\mathrm{i}}{\hbar}\left[\hat{H}_{\mathrm{int}}(t), \hat{a}^\dagger_{s,H}\,\hat{a}_{s,H}\right]\right\rangle, \tag{17}$$

The commutator is easily calculated, leading to

$$\frac{\mathrm{d}}{\mathrm{d}t}\left(\hat{\mathcal{N}}\right)_\rho = -\frac{2}{\hbar}\mathrm{Im}\left\{\left(\hat{\mathcal{E}}(\mathbf{r},t)\hat{V}^\dagger\right)_\rho\right\}. \tag{18}$$

The density operator at time t can be expressed starting with the initial ($t\to-\infty$) density operator whose matter and field degrees of freedom are uncoupled, which is then propagated by the Hamiltonian Equation (9). This propagation is most compactly described in terms of Liouville space "left" and "right" superoperators (Harbola & Mukamel, 2008; Mukamel, 2003; Cohen & Mukamel, 2003) which provide a clean bookkeeping device for all interactions. These are defined as

$$\begin{aligned}\hat{A}_{\mathrm{L}}\,\hat{X} &\equiv \hat{A}\,\hat{X},\\ \hat{A}_{\mathrm{R}}\hat{X} &\equiv \hat{X}\,\hat{A}\,.\end{aligned} \tag{19}$$

$\hat{A}_{\mathrm{L}}(\hat{A}_{\mathrm{R}})$ corresponds to an $\hat{A}$ appearing to the left (right) of $\hat{X}$ in Hilbert space. We further introduce linear combinations of L/R operations, which will be referred to as $+/-$ operations

$$\hat{A}_\pm \equiv \frac{1}{\sqrt{2}}\left[\hat{A}_{\mathrm{L}} \pm \hat{A}_{\mathrm{R}}\right]. \tag{20}$$

$\hat{A}_{\mathrm{L}}$, $\hat{A}_{\mathrm{R}}$, or equivalently $\hat{A}_+$, $\hat{A}_-$, form complete sets of superoperators which are connected by a unitary transformation.

Propagating $\hat{\rho}(t)$ by solving the Liouville equation $\frac{\mathrm{d}\hat{\rho}}{\mathrm{d}t} = -\frac{\mathrm{i}}{\hbar}\left[\hat{H},\hat{\rho}\right]$ gives (Marx et al., 2008; Roslyak et al., 2009)

$$\frac{\mathrm{d}}{\mathrm{d}t}\left(\hat{\mathcal{N}}\right)_\rho = -\frac{2}{\hbar}\Im\left[\left\langle \mathcal{T}\hat{\mathcal{E}}_{\mathrm{L}}(\mathbf{r},t)\hat{V}^\dagger_{\mathrm{L}}(t)\exp\left\{-\frac{\mathrm{i}}{\hbar}\int_{-\infty}^{t}\mathrm{d}\tau\sqrt{2}\mathcal{H}_{\mathrm{int}-}(\tau)\right\}\right\rangle\right]. \tag{21}$$

This together with Equation (14) or (16) provides an exact compact formal expression for the signals. A key ingredient in Equation (21) is the time ordering operator in Liouville space $\mathcal{T}$ which reorders superoperators so that ones with earlier times appear to the right of those with later time variables. Thanks to this operator we can use an ordinary exponent in Equation (21) without worrying about time ordering.

In the following we ignore spontaneous signals and focus solely on stimulated processes. We assume that the field is initially in a coherent state,

$$|\Psi_F\rangle = \exp\left(-\sum_s |\alpha_s|^2\right)\exp\left\{\sum_s \hat{a}_s^\dagger \alpha_s\right\}|0\rangle. \tag{22}$$

In Equation (22) α_s is the eigenvalue of the photon annihilation operator $\hat{a}_s$, $\hat{a}_s|\Psi_F\rangle=\alpha_s|\Psi_F\rangle$, and $|0\rangle$ is the vacuum state of the field. The expectation value of the field is then

$$\langle\Psi_F|\hat{E}(\mathbf{r},t)|\Psi_F\rangle=\mathcal{E}(\mathbf{r},t)+c.c., \tag{23}$$

where

$$\mathcal{E}(\mathbf{r},t)=\sum_s\left(\frac{2\pi\hbar\omega_s}{\Omega}\right)^{1/2} e^{i\mathbf{k}_s\cdot\mathbf{r}-i\omega_s t}\alpha_s, \tag{24}$$

is the field amplitude at space-point $\mathbf{r}$. Using Equation (22) the field expectation values can be calculated by simply replacing $\hat{\mathcal{E}}$ everywhere with its classical expectation value $\mathcal{E}(\mathbf{r},t)$.

Equation (21) contains all orders in the fields and can serve as a starting point for a perturbative calculation of specific signals. These are generally given by products of correlation functions of field and matter degrees of freedom. The different terms in the perturbative expansion of Equation (21) represent the various possible optical signals. These are conveniently described in terms of the loop diagrams which will be presented in Section 4.

3. TRANSITION-AMPLITUDES AND THE OPTICAL THEOREM FOR TIME-DOMAIN MEASUREMENTS

We wish to study optical signals from the viewpoint of the molecule, rather than the field, with the ultimate goal of relating the signals to material processes. This will be done in this section by recasting the signals in terms of transition amplitudes which originate from the perturbation theory of the molecular wave functions.

We start by considering a time-domain setup where the molecule interacts with a finite optical pulse. Namely, $E(\tau)\neq 0$ only for $t_0<\tau<t$, where t_0 is an initial time and t a final time, see Figure 3. From the material perspective, the quantity of interest is the probability to find the system at a final state c given that it was initially in state a

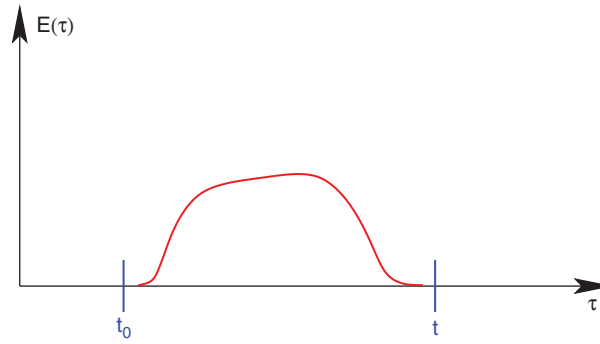

Figure 3 A time-domain experiment where a molecule interacts with a pulse (or a series of pulses) for a finite time, between an initial time, t_0, and a final time t

$$P_{a\to c} = \left|\langle c(t)|\hat{\mathcal{U}}(t,t_0)|a(t_0)\rangle\right|^2, \tag{25}$$

where $\hat{\mathcal{U}}(t,t_0) = \exp_+\left[-\frac{\mathrm{i}}{\hbar}\int_{t_0}^{t}\mathrm{d}\tau\mathcal{H}_I'(\tau)\right]$ is the time evolution operator in the interaction picture with respect to $\mathcal{H}_0$,

$$\mathcal{H}_I'(\tau) = U_0^{\dagger}(\tau,t_0)\mathcal{H}'(\tau)U_0(\tau,t_0).$$

U_0 is the evolution operator of the non-interacting field and matter, while $|a(t)\rangle\equiv U_0^{\dagger}(t,t_0)|a\rangle$. The time-ordered exponential is defined as

$$\exp_+\left[-\frac{\mathrm{i}}{\hbar}\int_{t_0}^{t}\mathrm{d}\tau\mathcal{H}_I'(\tau)\right] = 1+\sum_{n=1}^{\infty}\left(-\frac{\mathrm{i}}{\hbar}\right)^n\int_{t_0}^{t}\mathrm{d}\tau_n\int_{t_0}^{\tau_n}\mathrm{d}\tau_{n-1}\cdots\int_{t_0}^{\tau_2}\mathrm{d}\tau_1\mathcal{H}_I'(\tau_n)\mathcal{H}_I'(\tau_{n-1})\cdots\mathcal{H}_I'(\tau_1). \tag{26}$$

$\hat{\mathcal{U}}$ satisfies the integral equation

$$\hat{\mathcal{U}}(t,t_0) = 1-\frac{\mathrm{i}}{\hbar}\int_{t_0}^{t}\mathrm{d}\tau\mathcal{H}_I'(\tau)\hat{\mathcal{U}}(\tau,t_0), \tag{27}$$

which allows to recast its matrix elements in the form

$$\langle c(t)|\hat{\mathcal{U}}(t,t_0)|a(t_0)\rangle = \delta_{ca}\mathrm{e}^{-\frac{\mathrm{i}}{\hbar}\varepsilon_a(t-t_0)} - \frac{\mathrm{i}}{\hbar}\mathrm{e}^{-\frac{\mathrm{i}}{\hbar}(\varepsilon_c t-\varepsilon_a t_0)}T_{ca}(\omega_{ca}), \tag{28}$$

with $\hbar\omega_{ca} = \varepsilon_c - \varepsilon_a$,

$$T_{ca}(\omega) = \int \mathrm{d}t\ \mathrm{e}^{\mathrm{i}\omega\tau}\mathbb{T}_{ca}(\tau), \tag{29}$$

and

$$\mathbb{T}_{ca}(\tau) \equiv \langle c(\tau)|\mathcal{H}_I'(\tau)\exp_+\left[-\frac{\mathrm{i}}{\hbar}\int_{t_0}^{\tau}\mathrm{d}\tau'\mathcal{H}_I'(\tau')\right]|a(t_0)\rangle \mathrm{e}^{\frac{\mathrm{i}}{\hbar}\varepsilon_a(\tau-t_0)} \tag{30}$$

are the *transition amplitudes.*

Conservation of probability, or equivalently, unitarity of $\hat{\mathcal{U}}$, implies that $\sum_c \left|\hat{\mathcal{U}}_{ca}\right|^2 = 1$. Substitution of Equation (28) in this relation leads to the *optical theorem*

$$\Im T_{aa}(\omega_{aa}=0) = -\frac{1}{2\hbar}\sum_c |T_{ca}(\omega_{ca})|^2, \tag{31}$$

where T_{aa} is given by Equation (30) with $c(\tau)$ replaced by $a(\tau)$. The c summation runs over all states including c=a. This is analogous but different from the optical theorem of stationary (steady state) scattering theory (Newton, 1982), since here we consider pulsed excitation and the T matrix Equation (30) carries the full-time dependence of the fields.

Expanding Equation (31) in powers of the field gives

$$\begin{aligned} T_{ca}(\omega_{ca}) = &-\int \mathrm{d}\omega \mathcal{E}(\omega)\tilde{T}_{ca}^{(1)}(\omega)\delta(\omega_{ca}-\omega) \\ &+\frac{1}{2\pi\hbar}\int \mathrm{d}\omega_1\mathrm{d}\omega_2\mathcal{E}(\omega_1)\mathcal{E}(\omega_2)\tilde{T}_{ca}^{(2)}(\omega_2,\omega_1)\delta(\omega_{ca}-\omega_1-\omega_2) \\ &-\frac{1}{4\pi^2\hbar^2}\int \mathrm{d}\omega_1\mathrm{d}\omega_2\mathrm{d}\omega_3\mathcal{E}(\omega_1)\mathcal{E}(\omega_2)\mathcal{E}(\omega_3) \\ &\times\tilde{T}_{ca}^{(3)}(\omega_3,\omega_2,\omega_1)\delta(\omega_{ca}-\omega_1-\omega_2-\omega_3)+\cdots \end{aligned} \tag{32}$$

where

$$\tilde{T}_{ca}^{(1)}(\omega_1) \equiv \mu_{ca}, \tag{33}$$

$$\tilde{T}_{ca}^{(2)}(\omega_2,\omega_1) \equiv \sum_\nu \frac{\mu_{c\nu}\mu_{\nu a}}{\omega_1-\omega_{\nu a}+\mathrm{i}\eta}, \tag{34}$$

$$\tilde{T}_{ca}^{(3)}(\omega_3,\omega_2,\omega_1) \equiv \sum_{\nu_1,\nu_2} \frac{\mu_{c\nu_2}\mu_{\nu_2\nu_1}\mu_{\nu_1 a}}{(\omega_1+\omega_2-\omega_{\nu_2 a}+\mathrm{i}\eta)(\omega_1-\omega_{\nu_1 a}+\mathrm{i}\eta)} \tag{35}$$

and so forth.

The *partial transition amplitudes* $\tilde{T}$ introduced above are defined as follows: (i) each transition between states contributes a dipole operator μ

factor, (ii) propagation between transitions is given by a Green's function whose argument is the cumulative frequencies of field modes, minus the transition frequency between the current and initial state. These quantities can also be used in a frequency-domain setup.

As an example, a second-order transition from a to c through ν, which involve absorption of ω_1 and then ω_2 would be described by

$$\tilde{T}^{(2)}_{ca}(\omega_2,\omega_1)=\frac{\mu_{c\nu}\mu_{\nu a}}{\omega_1-\omega_{\nu a}+\mathrm{i}\eta},$$

where η is a positive infinitesimal. Each transition amplitude describes a partial contribution of a specific molecular process. The partial amplitudes are multiplied by the field amplitudes and summed over to give the full transition amplitude of the process, see Equation (32).

We shall denote quantities such as $\tilde{T}^{(2)}_{ca}(\omega_2,\omega_1)$, that do not include the field amplitudes, as *bare* transition amplitudes as opposed to the *dressed* (partial) transition amplitudes which include the fields as well. The two are related by $T^{(2)}_{ca}(\omega_2,\omega_1)=\mathcal{E}_1\mathcal{E}_2\tilde{T}^{(2)}_{ca}(\omega_2,\omega_1)$ etc. We will mostly use bare amplitudes in what follows. To distinguish these partial amplitudes from the full transition amplitudes of Equation (30), they contain a superscript that denotes their order in the field–matter interaction.

The optical theorem (31) can be represented diagrammatically. The expansion Equation (32) of the transition amplitude is depicted schematically in Figure 4. The summation in Figure 4 corresponds to that of Equation (32), namely a sum over all intermediate states and all frequency combinations which sum to ω (with negative signs for emission). With the help of the diagrammatic representation of $T_{\mathrm{ca}}(\omega)$, the optical theorem (31) is depicted in Figure 5.

The rates of various material processes can be expressed using the transition amplitudes. In a frequency-domain measurement the rate of a k-photon process assumes the generalized Kramers-Heisenberg form

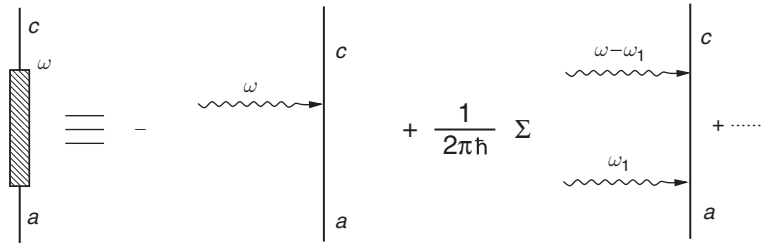

Figure 4 Diagrammatic representation of the transition amplitude $T_{\mathrm{ca}}(\omega)$ [Equation (32)]

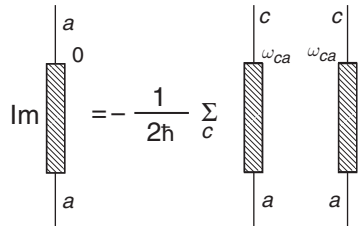

Figure 5 Diagrammatic representation of Equation (31). The two strands on the right-hand side correspond to the evolution of the ket and the bra, and are complex conjugates of each other

$$R_{a\to c} \propto \left|T_{ca}^{(k)}(\omega_1,\ldots,\omega_k)\right|^2 \delta\left(\sum_{i=1}^{k}\omega_k - \omega_{ca}\right).$$

This process makes the following contribution to an optical signal where photon i is detected

$$S_i \sim AR_{a\to c}.$$

Here $A = +1$ if the photon ω_i is emitted, -1 if it is absorbed, and 0 if it is neither absorbed or emitted. The generalization to processes where more than one photon is emitted or absorbed is obvious.

The discussion in the previous section assumed that a single-field pathway contributes to the molecular transition. When several pathways are possible they must be added at the amplitude level (as in Figure 2) and will interfere

$$\Delta N_{a\to c} \propto \left|T_{ca}^{(k_1)}(\omega_1,\ldots,\omega_{k_1})\delta\left(\sum_{i=1}^{k_1}\omega_i - \omega_{ca}\right)\right.$$
$$\left. + T_{ca}^{(k_2)}(\omega_{k_1+1},\ldots,\omega_{k_1+k_2})\delta\left(\sum_{i=k_1+1}^{k_1+k_2}\omega_i - \omega_{ca}\right)\right|^2.$$

By expanding the brackets we see that terms of the form $\left[T_{ca}^{(k_1)}T_{ca}^{(k_2)*} + c.c\right]\delta\left(\Sigma_{i=1}^{k_1}\omega_i - \omega_{ca}\right)\delta\left(\Sigma_{i=k_1+1}^{k_1+k_2}\omega_i - \omega_{ca}\right)$ can be interpreted as an interference correction for the number of molecular transitions.[1] A similar interpretation holds also for optical signals.

By recasting the optical signal in one of the above forms it can be interpreted in terms of the underlying molecular transitions. This is

[1]The appearance of factor of δ^2 once the bracket is squared reflects the fact that the diagonal terms are naturally described in terms of the rate of a process, while non-diagonal terms are described in terms of the overall number of transitions. We will clarify this for CARS signals in Section 9.

straightforward for pump–probe processes but is less obvious for CARS, due to the existence of parametric processes, which contribute to optical signals but do not represent a molecular process since they eventually leave the molecule at its initial state.

3.1 Purely Dissipative Signals

Optical signals generally include contributions from two types of processes: resonant, where the matter makes a transition from one state to another, and parametric, where photons are exchanged between different field modes, but the molecule only serves as a "catalyst" and ultimately returns to its initial state. The latter typically give a broad, featureless, background to optical signals and the resonant signal from the molecule of interest may be masked by a much stronger parametric background from, for example, solvent molecules (Kirkwood et al., 2000). Removing the parametric background is of great interest for spectroscopic and imaging applications (Li et al., 2008; Pestov et al., 2008; Potma et al., 2006). Based on our analysis, this can generally be accomplished by measuring the total energy exchanged between the field and matter. This *dissipative signal* requires detecting *all* the field modes as is given by $-\Sigma_i \omega_i S_i$, where S_i is the signal in the ith mode and may be easily calculated from the material perspective as

$$D = \int \mathrm{d}\omega D(\omega), \tag{36}$$

$$D(\omega) \equiv \hbar^{-1} \sum_{fg} P(g)\omega |T_{fg}(\omega)|^2 \delta(\omega - \omega_{fg}). \tag{37}$$

$D(\omega)$ is the energy gained by the material through transitions between states separated by energy $\hbar\omega$. Note that ω can be any combination of field frequencies.

D may be measured by subtracting the transmitted and incoming pulse energies. Parametric processes do not affect the total field energy and thus do not contribute to D. Obviously, D will be useful as a spectroscopic tool provided that specific resonances can be separated out by varying pulse parameters. We will return to this point in Section 10.

4. CTPL REPRESENTATION OF OPTICAL SIGNALS

In the following sections we apply the transition amplitude approach to calculate the pump–probe and CARS signals. These signals, which are fourth order in the field, will be calculated diagrammatically by expanding Equation (21), assuming that the field is initially in a coherent state [Equation (22)].

The contribution of each diagram could be read out following the rules given below. The diagrams represent the expansion of the ordered exponential in Equation (21). Note that only the imaginary part of the diagrams contributes to the signals.

There are several types of diagrams, which differ by the bookkeeping of matter–field interactions. Time-domain measurements are commonly represented by double-sided Feynman diagrams for the density matrix (Mukamel, 1995, 2008). Only forward time evolution is required in that case. These diagrams are read from bottom to top following the evolution of both the ket and the bra in the physical time. They are well documented and we will not repeat their description here. Suffice it to note that these diagrams maintain full bookkeeping of the time ordering, namely that all interactions are ordered in time, whether they are with the ket or with the bra, this makes them particularly suitable for time-domain measurements.

The loop diagrams presented below, in contrast, are not read in real (physical) time, but rather clockwise along the loop: time first runs forward on the left branch (ket) and then backwards on the right branch (bra). The interactions are ordered along the loop. Loop diagrams are therefore partially ordered in real time. (Only interactions in each branch are time ordered.) This turns out to be most convenient for frequency-domain techniques, where no specific order of interactions is enforced by the field envelopes. Fewer loop diagrams are required since each loop diagram represents a sum of several double-sided Feynman diagrams which reflect all possible time orderings of interactions on the ket and bra following (Marx et al., 2008). We now present the rules used to read these diagrams. These will then be used to calculate the pump–probe [Equation (39)] and the CARS [Equation (59)] signals. Hereafter we only use the FD rules but for completeness we also give the rules in the time domain. Example of an application of the time domain rules can be found in Marx et al. (2008).

4.1 Rules for the CTPL Diagrams in the Time Domain

TD1 The loop represents the density operator. Its left branch stands for the ket, the right corresponds to the bra.

TD2 Each interaction with a field mode is represented by a wavy line on either the right (R-superoperators) or the left (L-superoperators) branch.

TD3 The field is indicated by dressing the wavy lines with arrows, where an arrow pointing to the right represents the field annihilation operator $\mathcal{E}(\mathbf{r},t)$, which involves the term $e^{i(k_j\cdot\mathbf{r}-\omega_j t)}$ (see Equation (12)). Conversely, an arrow pointing to the left corresponds to the field creation operator $\mathcal{E}^{\dagger}(\mathbf{r},t)$, associated with a $e^{-i(k_j\cdot\mathbf{r}-\omega_j t)}$ factor. This is made explicit by adding the wave vectors $\pm\mathbf{k}_j$ to the arrows.

TD4 Within the RWA, each interaction with $\mathcal{E}(\mathbf{r},t)$ is accompanied by applying the operator $V^{\dagger}$, which leads to excitation of the state represented by the ket and de-excitation of the state represented by the bra, respectively. Arrows pointing "inwards" (i.e., pointing to the right on the ket and to the left on the bra) consequently cause absorption of a photon by exciting the system, whereas arrows pointing "outwards" (i.e., pointing to the left on the bra and to the right on the ket) represent de-exciting the system by photon emission.

TD5 The interaction at the observation time t is always the last. As a convention, it is chosen to occur from the left. This choice is arbitrary and does not affect the result.

TD6 Interactions within each branch are time ordered, but interactions on different branches are not. Each loop can be further decomposed into several fully-time-ordered diagrams (double-sided Feynman diagrams). These can be generated from the loop by simply shifting the arrows along each branch, thus changing their position relative to the interactions on the other branch. Each of these relative positions then gives rise to a particular fully-time-ordered diagram.

TD7 The overall sign of the correlation function is given by $(-1)^{N_{\mathrm{R}}}$, where N_{R} stands for the number of interactions from the right.

TD8 Diagrams representing $(n+1)$-wave mixing acquire a common prefactor i^{n}.

4.2 Rules for the CTPL Diagrams in the Frequency Domain

FD1 Time runs along the loop clockwise from bottom left to bottom right.

FD2 Each interaction with a field mode is represented by a wavy line.

FD3 The field is indicated by dressing the wavy lines with arrows, where an arrow pointing to the right represents the field annihilation operator $\mathcal{E}(\mathbf{r},t)$, which involves the factor $\mathrm{e}^{\mathrm{i}(\mathbf{k}_s\cdot\mathbf{r}-\omega_s t)}$. Conversely, an arrow pointing to the left corresponds to the field creation operator $\mathcal{E}^{\dagger}(\mathbf{r},t)$, being associated with $\mathrm{e}^{-\mathrm{i}(\mathbf{k}_s\cdot\mathbf{r}-\omega_s t)}$. This is made explicit by adding the wave vectors $\pm\mathbf{k}_s$ to the arrows.

FD4 Within the RWA each interaction with $\mathcal{E}(\mathbf{r},t)$ is accompanied by applying the operator $V^{\dagger}$, which leads to excitation of the material system. Arrows pointing to the right cause absorption of a photon by exciting the molecule, whereas arrows pointing to the left represent de-exciting the system by photon emission.

FD5 The interaction at the observation time t is fixed to be with the detected mode and is always the last. It is chosen to occur on the left branch of the loop. This choice is arbitrary and does not affect the result.

FD6 The loop translates into an alternating product of interactions (arrows) and periods of free evolutions (vertical solid lines) along the loop.

FD7 Since the loop time goes clockwise along the loop, periods of free evolution on the left branch amount to propagating forward in real time ($iG(\omega)$), whereas evolution on the right branch corresponds to backward propagation ($-iG^{\dagger}(\omega)$).

FD8 The frequency arguments of the various propagators are cumulative, i.e. they are given by the sum of all "earlier" interactions along the loop. Additionally, the ground state frequency ω_g is added to all arguments of the propagators.

FD9 A diagram representing $n+1$ mixing caries the prefactor $i^n(-1^{N_R})$(N_R is the number of interactions from the right).

5. THE PUMP–PROBE SIGNAL

Pump–probe is the simplest nonlinear technique: the system interacts with two fields, a pump $\mathbf{k}_1$, and a probe $\mathbf{k}_2$ (which is detected). The signal is defined as the difference in the probe transmitted intensity between measurements where the pump is present or absent. This difference between two large quantities amounts to "determining the weight of the captain by weighting the ship with and without the captain". It limits the sensitivity compared to homodyne four-wave mixing signals. However, this technique is simpler to implement and does not require phase control of the pulses. Stimulated Raman spectroscopy (Alfano & Shapiro, 1971; Jones & Stoicheff, 1964) carried out with a combination of broadband (femtosecond) and narrowband (picosecond) pulses is widely used for improving the sensitivity of spontaneous Raman signals (Laimgruber et al., 2006; Lakshmanna, 2009; Mallick et al., 2008; Wilson et al., 2009). This technique has also been used for bioimaging applications (Min et al., 2009).

We shall calculate the frequency-domain pump–probe signal starting from Equation (16). We assume that the field intensities are high enough so that spontaneous emission can be safely neglected and all matter/field interactions are stimulated. The derivation starts by using Equation (16) and expanding the exponent in Equation (21) to third order,

$$S_{PP} = -\frac{1}{3\hbar^4}\mathrm{Re}\int\int\int_{-\infty}^{t} d\tau_1 d\tau_2 d\tau_3 \mathcal{E}_2(t) \times \langle \mathcal{T}\hat{V}_L^{\dagger}(t)\mathcal{H}_{int-}(\tau_1)\mathcal{H}_{int-}(\tau_2)\mathcal{H}_{int-}(\tau_3)\rangle. \quad (38)$$

Only contributions proportional to $|\mathcal{E}_1|^2|\mathcal{E}_2|^2$ where two of the interactions are with the probe, and two are with the pump, will be kept. For these contributions the expectation value in Equation (38) turns out to be independent of t. This is the reason for using Equation (16) to define the signal. An additional integration over t would result in an infinite signal.

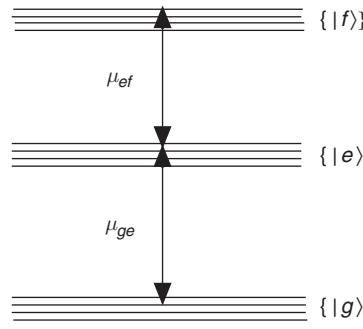

Figure 6 The three-band (ladder) model system and transition dipoles used in the derivation of Equation (39)

We will consider the three-band model, as depicted in Figure 6. Within the RWA we neglect off-resonant contributions and only retain the resonant ones where photon absorption is accompanied by a molecular-up transition and vice versa. This excellent approximation for resonant signals limits the number of possible processes and simplifies the analysis. For instance, it excludes emission from the ground state band, as well as three consecutive absorptions. Substitution of $\mathcal{H}_{\text{int}-}$ in Equation (38) results in the eight terms (Roslyak et al., 2009), which are depicted diagrammatically in Figure 7. The frequency-domain signal (absorption of ω_2), which can be read from the diagrams with the help of the rules in Section 4.2, is given by

$$\begin{aligned}
S_{\text{PP}}(\omega_2;\omega_1) = -\frac{4}{\hbar^4}|\mathcal{E}_1|^2|\mathcal{E}_2|^2 \\
\times \text{Im}\Big\{ &\langle \hat{V}\hat{G}^\dagger(\omega_g+\omega_1)\hat{V}\hat{G}^\dagger(\omega_g+\omega_1+\omega_2)\hat{V}^\dagger\hat{G}(\omega_g+\omega_1)\hat{V}^\dagger\rangle \\
&+\langle \hat{V}\hat{G}^\dagger(\omega_g+\omega_2)\hat{V}\hat{G}^\dagger(\omega_g+\omega_1+\omega_2)\hat{V}^\dagger\hat{G}(\omega_g+\omega_1)\hat{V}^\dagger\rangle \\
&+\langle \hat{V}\hat{G}^\dagger(\omega_g+\omega_1)\hat{V}\hat{G}^\dagger(\omega_g+\omega_1+\omega_2)\hat{V}^\dagger\hat{G}^\dagger(\omega_g+\omega_2)\hat{V}^\dagger\rangle \\
&+\langle \hat{V}\hat{G}^\dagger(\omega_g+\omega_2)\hat{V}\hat{G}^\dagger(\omega_g+\omega_1+\omega_2)\hat{V}^\dagger\hat{G}^\dagger(\omega_g+\omega_2)\hat{V}^\dagger\rangle \\
&+\langle \hat{V}\hat{G}^\dagger(\omega_g+\omega_2)\hat{V}^\dagger\hat{G}(\omega_g+\omega_1-\omega_1)\hat{V}\hat{G}(\omega_g+\omega_1)\hat{V}^\dagger\rangle \\
&+\langle \hat{V}\hat{G}^\dagger(\omega_g+\omega_1)\hat{V}^\dagger\hat{G}^\dagger(\omega_g+\omega_2-\omega_2)\hat{V}\hat{G}^\dagger(\omega_g+\omega_2)\hat{V}^\dagger\rangle \\
&+\langle \hat{V}\hat{G}^\dagger(\omega_g+\omega_2)\hat{V}^\dagger\hat{G}^\dagger(\omega_g+\omega_2-\omega_1)\hat{V}\hat{G}^\dagger(\omega_g+\omega_2)\hat{V}^\dagger\rangle \\
&-\Big\langle \hat{V}\hat{G}^\dagger(\omega_g+\omega_1)\hat{V}^\dagger\hat{G}^\dagger(\omega_g+\omega_1-\omega_2)\hat{V}\hat{G}(\omega_g+\omega_1)\hat{V}^\dagger\Big\rangle\Big\}. \quad (39)
\end{aligned}$$

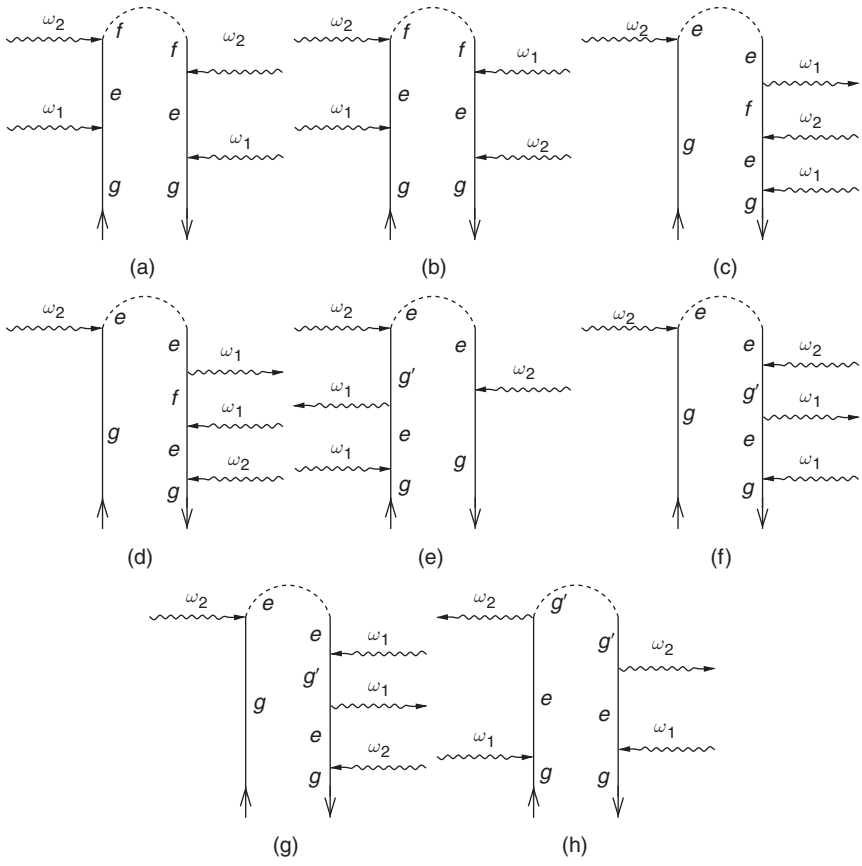

Figure 7 CTPL diagrams for the eight contributions to the pump–probe signal, respectively [Equation (39)]

Here $\hat{G}(\omega) = (\omega - H_0 + \mathrm{i}\eta)^{-1}$ is the retarded Green's function and $\hat{G}^{\dagger}(\omega) = (\omega - H_0 - \mathrm{i}\eta)^{-1}$ is the advanced Green's function.

The terms in Equation (39) naturally separate into two groups depending on the order of absorption and emission events *along the loop*. The first four terms have two consecutive absorptions followed by two emissions ($VVV^{\dagger}V^{\dagger}$), and the matter goes through the doubly excited f band. These contributions will therefore be termed two–photo absorption (TPA). Terms 5–8 have the form of absorption, emission, absorption, emission ($VV^{\dagger}VV^{\dagger}$) and only involve the g and e bands. These will be termed stimulated Raman scattering (SRS).

Expanding Equation (39) in the eigenvalues results in the final expression for the pump–probe signal

$$S_{\mathrm{PP}}(\omega_2;\omega_1) = S_{\mathrm{TPA}}(\omega_2;\omega_1) + S_{\mathrm{SRS}}(\omega_1;\omega_1), \tag{40}$$

with the two photon absorption component

$$\begin{aligned} S_{\mathrm{TPA}}(\omega_2;\omega_1) =& -4\pi N\hbar^{-4}|\mathcal{E}_1|^2|\mathcal{E}_2|^2|\mu_{eg}|^2|\mu_{fe}|^2\Im\sum_{g,g',e,f} \\ &\times\Bigg\{\frac{1}{(\omega_1-\omega_{eg}-\mathrm{i}\eta)(\omega_2+\omega_1-\omega_{fg}-\mathrm{i}\eta)(\omega_1-\omega_{eg}+\mathrm{i}\eta)} \\ &+\frac{1}{(\omega_2-\omega_{eg}-\mathrm{i}\eta)(\omega_2+\omega_1-\omega_{fg}-\mathrm{i}\eta)(\omega_1-\omega_{eg}+\mathrm{i}\eta)} \\ &+\frac{1}{(\omega_2-\omega_{eg}-\mathrm{i}\eta)(\omega_2+\omega_1-\omega_{fg}-\mathrm{i}\eta)(\omega_2-\omega_{eg}-\mathrm{i}\eta)} \\ &+\frac{1}{(\omega_2-\omega_{eg}-\mathrm{i}\eta)(\omega_1+\omega_2-\omega_{fg}-\mathrm{i}\eta)(\omega_1-\omega_{eg}-\mathrm{i}\eta)}\Bigg\}, \end{aligned} \tag{41}$$

and the stimulated Raman component

$$\begin{aligned} S_{\mathrm{SRS}}(\omega_2;\omega_1) =& \,4\pi N\hbar^{-4}|\mathcal{E}_1|^2|\mathcal{E}_2|^2\Im\sum_{g,g',e,f}|\mu_{eg}|^2|\mu_{g'e}|^2 \\ &\times\Bigg\{\frac{1}{(\omega_1-\omega_{eg}-\mathrm{i}\eta)(\omega_1-\omega_2-\omega_{g'g}-\mathrm{i}\eta)(\omega_1-\omega_{eg}+\mathrm{i}\eta)} \\ &-\frac{1}{(\omega_2-\omega_{eg}-\mathrm{i}\eta)(\omega_1-\omega_1-\omega_{g'g}-\mathrm{i}\eta)(\omega_1-\omega_{eg}-\mathrm{i}\eta)} \\ &-\frac{1}{(\omega_2-\omega_{eg}-\mathrm{i}\eta)(\omega_2-\omega_1-\omega_{g'g}-\mathrm{i}\eta)(\omega_2-\omega_{eg}-\mathrm{i}\eta)} \\ &-\frac{1}{(\omega_2-\omega_{eg}-\mathrm{i}\eta)(\omega_1-\omega_1-\omega_{g'g}+\mathrm{i}\eta)(\omega_1-\omega_{eg}+\mathrm{i}\eta)}\Bigg\}, \end{aligned} \tag{42}$$

Despite the straightforward derivation, it is not evident by a simple inspection of Equations (41) and (42) what are the material processes underlying the signal in real time since the calculation is done on a

loop that involves both forward and backward time evolutions. We emphasize that this bookkeeping along the loop merely gives the resonances that contribute to a particular signal, but since we are going forward and backward in time we cannot simply attribute a given loop diagram to a transition between an initial and a final state. This can only be done by breaking the loop into transition amplitudes and bringing them to the Kramers–Heisenberg form. This will be done next.

6. THE PUMP–PROBE SIGNAL REVISITED: TRANSITION AMPLITUDES

In this section the pump–probe signal will be dissected to reveal the underlying material processes. The dissection of signals into contributions corresponding to material processes is done by recasting the signals in terms of partial transition amplitudes. To that end we define slightly modified (frequency-domain) loop diagrams, termed unrestricted loop diagrams, that naturally represent material processes. The diagrams of Section 4 were aimed at the calculation of optical signals. The new diagrams, in contrast, correspond to generalized Kramers–Heisenberg terms, and therefore naturally represent the material processes.

6.1 Unrestricted Loop Diagrams

The unrestricted diagrams are closely related to those of Section 4.2, but with one difference: we drop the restriction that the last interaction from the left is at the latest time t, allowing for any relative time ordering between the last interactions on the ket and the bra. These will therefore be denoted unrestricted loop diagrams.

We will illustrate why the new diagrams are useful, and how to read them, using a simple example. The unrestricted diagram depicted in Figure 8 is given by the sum of two restricted loop diagrams where the last interaction is on either of the two branches of the loop. To distinguish between the two types of diagrams, we represent the unrestricted part of the loop by a solid line, as opposed to the dashed line used in the previous restricted diagrams. The two loop diagrams are read according to the rules of Section 4.2, omitting rule FD5 regarding the last interaction. From these rules, as well as our definition of partial transition amplitudes, the first diagram on the right-hand side of Figure 8 is proportional to $T_{ca}^{(1)}(\omega_1)T_{ca}^{(2)*}(\omega_3,\omega_2)\,(\omega_1-\omega_{ca}-\mathrm{i}\eta)^{-1}$. The second diagram on the right-hand side is similar, but with an opposite sign, and the advanced Green function $(\omega_1-\omega_{ca}-\mathrm{i}\eta)^{-1}$ is replaced by a retarded one $(\omega_1-\omega_{ca}+\mathrm{i}\eta)^{-1}$. (See rule FD7.) As a result, the contribution of the unrestricted loop diagram is proportional to

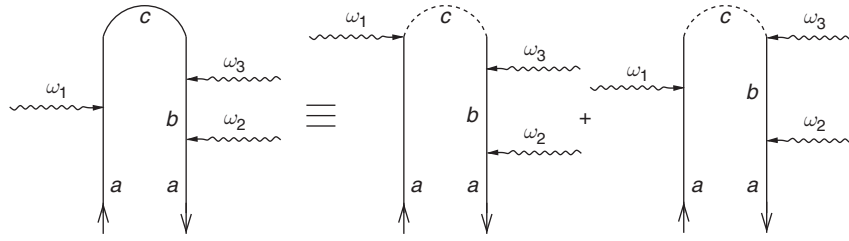

Figure 8 Example of an unrestricted loop diagram (solid line). The diagram is defined as the sum of two restricted diagrams, denoted by a dashed line along the top of the loop, where the last interaction is located either on the ket or on the bra. Phase matching requires $\omega_1 - \omega_2 - \omega_3 = 0$

$$\Im T_{ca}^{(1)}(\omega_1) T_{ca}^{(2)*}(\omega_3, \omega_2) \left[\frac{1}{\omega_1 - \omega_{ca} - \mathrm{i}\eta} - \frac{1}{\omega_1 - \omega_{ca} + \mathrm{i}\eta} \right]$$

$$= 2\pi \Re \left[T_{ca}^{(1)}(\omega_1) T_{ca}^{(2)*}(\omega_3, \omega_2) \right] \delta(\omega_1 - \omega_{ca}).$$

The reason for introducing the unrestricted diagrams now becomes clear: The contribution of such diagrams to the signal takes a generalized Kramers–Heisenberg form with the branches of the loop corresponding to partial transition amplitudes and the top of the loop to the resonant δ-function. These diagrams naturally connect optical signals with the underlying material processes.

While we used a simple example to demonstrate the definition and calculation of unrestricted diagrams, the generalization to any diagram is straightforward. There is only one class of special diagrams, namely ones where all interactions are either on the left branch or on the right branch, that needs to be treated separately. In this case there is no meaning to the relative ordering between branches, and we define the unrestricted diagrams to be equal to the restricted one. The contribution of such diagrams to the signal always takes the form $\sim \Im T_{aa}^{(n)}$, namely the imaginary part of a diagonal (partial) transition matrix. [See Figure 13(i) for an example.]

6.2 The Two-Photon-Absorption and Stimulated-Raman Components of the Pump-Probe Signal

We now dissect the pump–probe signal into contributions from various material processes. Equations (41) and (42) can be partially recast in terms of transition amplitudes by noting that the loop diagrams correspond to

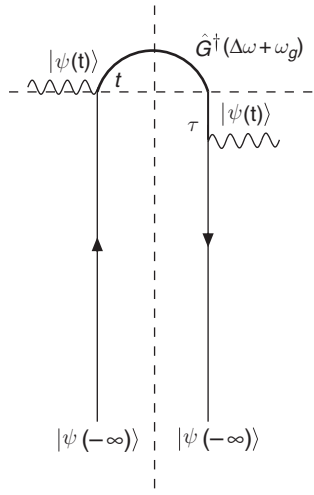

Figure 9 By dissecting the loop along its centerline it factorizes into two single-sided Feynman diagrams. This is possible since the system remains in the same state $\langle|\psi(t)\rangle$ between the topmost interaction on the two branches which occur, respectively, at times t and τ. The advanced propagator $\hat{G}^{\dagger}(\Delta\omega+\omega_g)$, representing backward propagation from t and τ, connects the two

the product of two such amplitudes times an additions propagator, as is explained in Figure 9. This allows to rewrite the signals as

$$S_{\mathrm{TPA}}(\omega_2;\omega_1) = -4\pi N\hbar^{-4}|\mathcal{E}_1|^2|\mathcal{E}_2|^2 \times\Im\sum_{g,g',e,f}\left(|\tilde{T}^{(2)}_{fg}(\omega_2,\omega_1)|^2+\tilde{T}^{(2)}_{fg}(\omega_2,\omega_1)\tilde{T}^{(2)*}_{fg}(\omega_1,\omega_2)\right)\frac{1}{\omega_2+\omega_1-\omega_{fg}-\mathrm{i}\eta} +\left(\tilde{T}^{(1)}_{eg}(\omega_2)\tilde{T}^{(3)*}_{eg}(-\omega_1,\omega_1,\omega_2)+\tilde{T}^{(1)}_{eg}(\omega_2)\tilde{T}^{(3)*}_{eg}(-\omega_1,\omega_2,\omega_1)\right)\frac{1}{\omega_2-\omega_{eg}-\mathrm{i}\eta}. \tag{43}$$

$$S_{\mathrm{SRS}}(\omega_2;\omega_1) = 4\pi N\hbar^{-4}|\mathcal{E}_1|^2|\mathcal{E}_2|^2\Im\sum_{g,g',e,f}\left|\tilde{T}^{(2)}_{g',g}(-\omega_2,\omega_1)\right|^2\frac{1}{\omega_1-\omega_2-\omega_{g'g}-\mathrm{i}\eta} -(\tilde{T}^{(1)}_{eg}(\omega_2)\tilde{T}^{(3)*}_{eg}(\omega_2,-\omega_1,\omega_1)+\tilde{T}^{(1)}_{eg}(\omega_2)\tilde{T}^{(3)*}_{eg}(\omega_1,-\omega_1,\omega_2) +\tilde{T}^{(3)}_{eg}(\omega_2,-\omega_1,\omega_1)\tilde{T}^{(1)*}_{eg}(\omega_2)\big)\frac{1}{\omega_2-\omega_{eg}-\mathrm{i}\eta}. \tag{44}$$

The first term corresponds to diagram (h) in Figure 7 whereas the second term is related to diagrams (e)–(g).

We start with the SRS signal (44). Taking the imaginary part of the first term results in a δ-function. The same is true for the sum of the second and fourth terms in Equation (44). Subtracting

$$\Im\left[\tilde{T}^{(3)}_{eq}(\omega_1,-\omega_1,\omega_2)\tilde{T}^{(1)*}_{eg}(\omega_2)\frac{1}{\omega_2-\omega_{eg}-\mathrm{i}\eta}\right.$$

$$\left.+\left|\tilde{T}^{(2)}_{g'g}(-\omega_1,\omega_2)\right|^2\frac{1}{\omega_2-\omega_1-\omega_{g'g}-\mathrm{i}\eta}\right]=0$$

from the terms in the sum in Equation (44) allows to bring all terms in Equation (44) to a form where the imaginary part can be taken, leading to various δ-functions. This gives

$$S_{\mathrm{SRS}}(\omega_2;\omega_1)=4\pi^2N\hbar^{-4}|\mathcal{E}_1|^2|\mathcal{E}_2|^2\sum_{gg'e}P(g)\left\{\left|\tilde{T}^{(2)}_{g'g}(-\omega_2,\omega_1)\right|^2\delta(\omega_1-\omega_2-\omega_{g'g})\right.$$

$$-\left|\tilde{T}^{(2)}_{g'g}(-\omega_1,\omega_2)\right|^2\delta(\omega_2-\omega_1-\omega_{g'g})$$

$$-\left[\tilde{T}^{(1)}_{eg}(\omega_2)\tilde{T}^{(3)*}_{eg}(\omega_1,-\omega_1,\omega_2)+c.c\right]\delta(\omega_2-\omega_{eg})$$

$$\left.-\left[\tilde{T}^{(1)}_{eg}(\omega_2)\tilde{T}^{(3)*}_{eg}(\omega_2,-\omega_1,\omega_1)+c.c\right]\delta(\omega_2-\omega_{eg})\right\}. \tag{45}$$

This has the desired generalized Kramers–Heisenberg form, allowing to identify the underlying molecular processes. The four terms in Equation (45) are represented diagrammatically by the unrestricted loop diagrams of Figure 10. For brevity we have omitted the diagrams corresponding to the two complex conjugate terms in Equation (45), but these can be easily obtained by reflecting diagrams (iii) and (iv) along a vertical line crossing the top of the loops.

Interestingly, all the terms proportional to $\delta(\omega_2-\omega_{\mathrm{eg}})$ could be combined into a single term whose amplitude is the sum of three processes, with corrections which have different scaling in the field amplitude. This gives

$$\tilde{S}_{\mathrm{SRS}}(\omega_2;\omega_1)=4\pi^2N\hbar^{-4}\sum_{g,g',e,f}|\mathcal{E}_1|^2|\mathcal{E}_2|^2|\tilde{T}^{(2)}_{g'g}(-\omega_2,\omega_1)|^2\delta(\omega_1-\omega_2-\omega_{g'g})$$

$$-|\mathcal{E}_1|^2|\mathcal{E}_2|^2|\tilde{T}^{(2)}_{g'g}(-\omega_1,\omega_2)|^2\delta(\omega_2-\omega_1-\omega_{g'g})$$

$$+|\mathcal{E}_2|^2|\tilde{T}^{(1)}_{eg}(\omega_2)|^2\delta(\omega_2-\omega_{eg})$$

$$- \left| \mathcal{E}_2 \tilde{T}^{(1)}_{eg}(\omega_2) + |\mathcal{E}_1|^2 \mathcal{E}_2 \tilde{T}^{(3)}_{eg}(\omega_1, -\omega_1, \omega_2) \right.$$

$$\left. + |\mathcal{E}_1|^2 \mathcal{E}_2 \tilde{T}^{(3)}_{eg}(\omega_2, -\omega_1, \omega_1) \right|^2 \delta(\omega_2 - \omega_{eg}). \tag{46}$$

where we have introduced an additional term to eliminate the $\sim |\mathcal{E}_2|^2$ part. The SRS signal is obtained from Equation (46) by neglecting terms of order $|\mathcal{E}_2|^2 |\mathcal{E}_1|^4$. Obviously, to obtain a Kramers–Heisenberg form we must give up the strict bookkeeping in orders of the field since that form naturally mixes the different orders.

We next turn to the TPA term. It can be brought to a form in which one can take the imaginary part, leading to δ-functions by adding to all terms in the sum of Equation (43)

$$\Im \left\{ \left[\left| \tilde{T}^{(2)}_{fg}(\omega_1, \omega_2) \right|^2 + \tilde{T}^{(2)}_{fg}(\omega_1, \omega_2) \tilde{T}^{(2)*}_{fg}(\omega_2, \omega_1) \right] \frac{1}{\omega_2 + \omega_1 - \omega_{fg} - \mathrm{i}\eta} \right.$$

$$\left. + \left[\tilde{T}^{(3)}_{eg}(-\omega_1, \omega_1, \omega_2) \tilde{T}^{(1)*}_{eg}(\omega_2) + \tilde{T}^{(3)}_{eg}(-\omega_1, \omega_2, \omega_1) \tilde{T}^{(1)*}_{eg}(\omega_2) \right] \frac{1}{\omega_2 - \omega_{eg} - \mathrm{i}\eta} \right\} = 0.$$

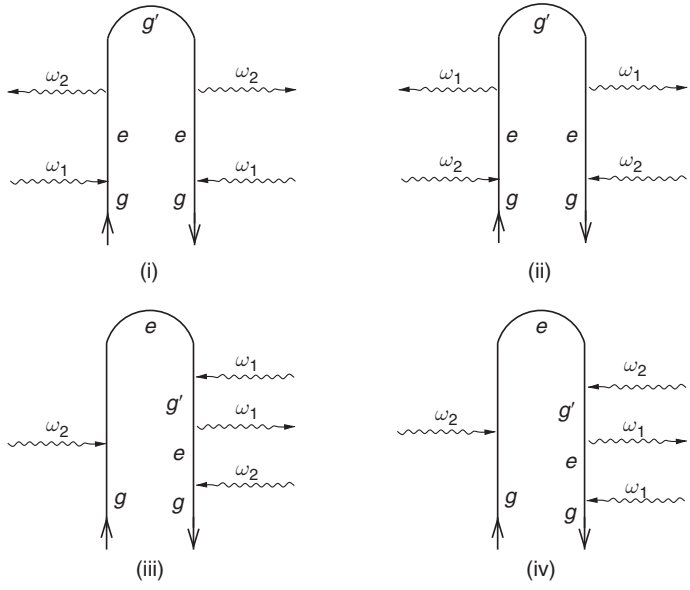

Figure 10 Unrestricted loop diagrams corresponding to the four terms in Equation (45), respectively

This leads to

$$S_{\mathrm{TPA}}(\omega_2;\omega_1) = -4\pi^2 N\hbar^{-4}|\mathcal{E}_1|^2|\mathcal{E}_2|^2 \times \sum_{gg'ef} P(g)\Big\{\Big|\tilde{T}^{(2)}_{fg}(\omega_2,\omega_1)+\tilde{T}^{(2)}_{fg}(\omega_1,\omega_2)\Big|^2\delta(\omega_1+\omega_2-\omega_{fg}) + \Big[\tilde{T}^{(1)}_{eg}(\omega_2)\tilde{T}^{(3)*}_{eg}(-\omega_1,\omega_1,\omega_2)+c.c.\Big]\delta(\omega_2-\omega_{eg}) + \Big[\tilde{T}^{(1)}_{eg}(\omega_2)\tilde{T}^{(3)*}_{eg}(-\omega_1,\omega_2,\omega_1)+c.c.\Big]\delta(\omega_2-\omega_{eg})\Big\}. \quad (47)$$

The terms of Equation (47) are depicted diagrammatically in Figure 11. The complex conjugates of the last two terms are omitted for brevity, as they are the mirror images of diagrams 11(ii) and 11(iii).

Combining the last two terms into one amplitude, as was done for the SRS signal, would give

$$\tilde{S}_{TPA}(\omega_2;\omega_1) = -4\pi^2 N\hbar^{-4}\sum_{g,g',e,f}|\mathcal{E}_1|^2|\mathcal{E}_2|^2|\tilde{T}^{(2)}_{fg}(\omega_2,\omega_1) + \tilde{T}^{(2)}_{fg}(\omega_1,\omega_2)|^2\delta(\omega_2+\omega_1-\omega_{fg}) + \Big|\mathcal{E}_2\tilde{T}^{(1)}_{eg}(\omega_2)+|\mathcal{E}_1|^2\mathcal{E}_2\tilde{T}^{(3)}_{eg}(-\omega_1,\omega_1,\omega_2) + |\mathcal{E}_1|^2\mathcal{E}_2\tilde{T}^{(3)}_{eg}(-\omega_1,\omega_2,\omega_1)\Big|^2\delta(\omega_2-\omega_{eg}) - |\mathcal{E}_2|^2|\tilde{T}^{(1)}_{eg}(\omega_2)|^2\delta(\omega_2-\omega_{eg}). \quad (48)$$

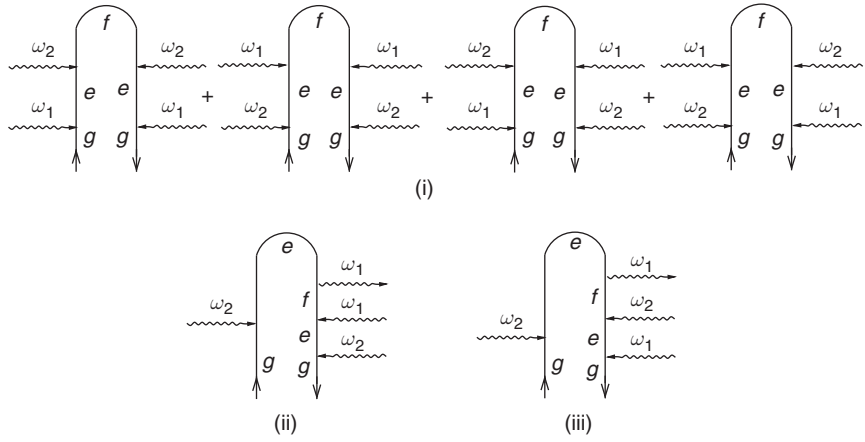

Figure 11 Unrestricted loop diagrams corresponding to the three terms in Equation (47), respectively

Again, Equation (47) can be obtained from Equation (48) by neglecting terms of order $|\mathcal{E}_2|^2|\mathcal{E}_1|^4$. We thus accomplished our goal of expressing the signal in a generalized Kramers-Heisenberg form.

7. COHERENT ANTI-STOKES RAMAN SPECTROSCOPY

Heterodyne CARS is a four-wave mixing technique where the system interacts with four field modes (Begley et al., 1974; Evans & Xie, 2008; Lotem et al., 1976; Penzkofer et al., 1979; Silberberg, 2009). The technique provides a powerful spectroscopic tool for probing molecular vibrations and for imaging applications (Nan et al., 2006; Potma & Xie, 2008; Potma et al., 2006). Time domain femtosecond techniques with pulse shaping have been employed to enhance the degree of control over the signals (Kukura et al., 2007; Laimgruber et al., 2006; Mallick et al., 2008; Mukamel, 2009; Oron et al., 2002; Pestov et al., 2007). We will start with the time-integrated signal (14). This is convenient since the CARS contributions, which interact once with each field, will depend on t through a factor of $\exp[i(\omega_1-\omega_2+\omega_3-\omega_4)t]$. (In the frequency-domain technique the field amplitudes are time independent.) The t integral then results in a factor of $2\pi\delta(\omega_1-\omega_2+\omega_3-\omega_4)$, giving a singular signal in the continuous wave (CW) limit. This further shows that only frequency combinations satisfying

$$\omega_1-\omega_2+\omega_3-\omega_4=0, \tag{49}$$

can contribute to the signal.

There are four possible CARS signals (Mukamel, 1995) which only differ by the choice of the detected mode. Denoting the signal obtained by measuring mode ω_i by S_i, we have

$$S_1=-\frac{4\pi}{\hbar}\delta(\omega_1-\omega_2+\omega_3-\omega_4)\Im\left[\mathcal{E}_1^*\mathcal{E}_2\mathcal{E}_3^*\mathcal{E}_4\chi^{(3)}(-\omega_1;\omega_4,-\omega_3,\omega_2)\right], \tag{50}$$

$$S_2=-\frac{4\pi}{\hbar}\delta(\omega_1-\omega_2+\omega_3-\omega_4)\Im\left[\mathcal{E}_1\mathcal{E}_2^*\mathcal{E}_3\mathcal{E}_4^*\chi^{(3)}(-\omega_2;\omega_3,-\omega_4,\omega_1)\right], \tag{51}$$

$$S_3=-\frac{4\pi}{\hbar}\delta(\omega_1-\omega_2+\omega_3-\omega_4)\Im\left[\mathcal{E}_1^*\mathcal{E}_2\mathcal{E}_3^*\mathcal{E}_4\chi^{(3)}(-\omega_3;\omega_2,-\omega_1,\omega_4)\right], \tag{52}$$

$$S_4=-\frac{4\pi}{\hbar}\delta(\omega_1-\omega_2+\omega_3-\omega_4)\Im\left[\mathcal{E}_1\mathcal{E}_2^*\mathcal{E}_3\mathcal{E}_4^*\chi^{(3)}(-\omega_4;\omega_1,-\omega_2,\omega_3)\right]. \tag{53}$$

The pump–probe technique only involves two field modes. The four field modes in CARS generate a larger number of terms. To keep the problem manageable, we employ the model of Figure 12 which limits the number of optical transitions. a and c are vibrational states belonging to the ground electronic state whereas b is an electronically excited state. Levels

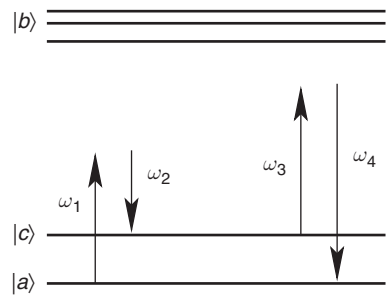

Figure 12 Level scheme and optical transitions for the CARS process

a and c are resonantly coupled by two possible Raman processes, with $\omega_1 - \omega_2 = \omega_4 - \omega_3 \simeq \omega_{ca}$. The system is described by the Hamiltonian (Mukamel, 1995; Scully & Zubairy, 1997; Shen, 2002)

$$\mathcal{H} = \mathcal{H}_{\rm s} + \mathcal{H}_{\rm f} + \mathcal{H}_{\rm int}, \tag{54}$$

with the molecular part

$$\mathcal{H}_{\rm s} = \hbar\omega_a|a\rangle\langle a| + \hbar\omega_b|b\rangle\langle b| + \hbar\omega_c|c\rangle\langle c|, \tag{55}$$

and the field part

$$\mathcal{H}_{\rm f} = \sum_{i=1}^{4} \hbar\omega_i \hat{a}_i^{\dagger}\,\hat{a}_i. \tag{56}$$

Within the RWA, the dipole coupling between the laser field and the molecule is given by

$$\mathcal{H}_{\rm int} = \left(\frac{2\pi\omega_1}{\Omega}\right)^{1/2} \hat{a}_1\,{\rm e}^{-{\rm i}\omega_1 {\rm t}}\mu_{ba}|b\rangle\langle a| + \left(\frac{2\pi\omega_2}{\Omega}\right)^{1/2} \hat{a}_2 {\rm e}^{-{\rm i}\omega_2 {\rm t}}\mu_{bc}|b\rangle\langle c|$$

$$+\left(\frac{2\pi\omega_3}{\Omega}\right)^{1/2} \hat{a}_3 {\rm e}^{-{\rm i}\omega_3 {\rm t}}\mu_{bc}|b\rangle\langle c| + \left(\frac{2\pi\omega_4}{\Omega}\right)^{1/2} \hat{a}_4 {\rm e}^{-{\rm i}\omega_4 {\rm t}}\mu_{ba}|b\rangle\langle a| + h.c. \tag{57}$$

The CTPL diagrams, which correspond to the two processes contributing to the signal (53) are depicted in Figure 13. In (*i*) the system is initially in the lower state a, while in (*ii*) it starts in the vibrationally excited state c. The loop diagrams can be read according to the rules given in Section 4, leading to

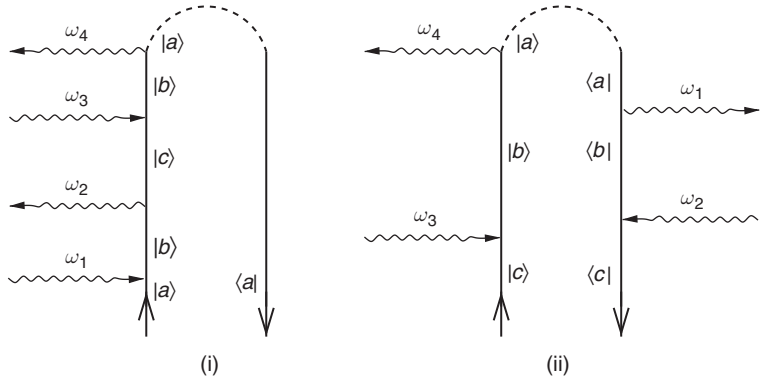

Figure 13 CTPL representation of $\chi^{(3)}(-\omega_4;\omega_1,-\omega_2,\omega_3)$ which is related to the S_4 signal. (i) and (ii) represent the two terms in Equation (58) respectively. In both the interaction with the detected mode (ω_4) is chronologically the last

$$\chi^{(3)}(-\omega_4;\omega_1,-\omega_2,\omega_3) = -\frac{|\mu_{ba}|^2|\mu_{cb}|^2}{\hbar^3}$$
$$\times\left[\frac{P(a)}{(\omega_1-\omega_2+\omega_3-\omega_{ba}+\mathrm{i}\eta)(\omega_1-\omega_2-\omega_{ca}+i\eta)(\omega_1-\omega_{ba}+\mathrm{i}\eta)}\right.$$
$$\left.+\frac{P(c)}{(\omega_3-\omega_4+\omega_1-\omega_{bc}-\mathrm{i}\eta)(\omega_3-\omega_4-\omega_{ac}-i\eta)(\omega_3-\omega_{bc}+\mathrm{i}\eta)}\right]. \quad (58)$$

Substitution in Equation (53) gives

$$S_4 = \frac{4\pi}{\hbar^4}\delta(\omega_1-\omega_2+\omega_3-\omega_4)\Im\left[\mathcal{E}_1\mathcal{E}_2^*\mathcal{E}_3\mathcal{E}_4^*|\mu_{ab}|^2|\mu_{bc}|^2\right.$$
$$\times\left(\frac{P(a)}{(\omega_4-\omega_{ba}+\mathrm{i}\eta)(\omega_1-\omega_2-\omega_{ca}+\mathrm{i}\eta)(\omega_1-\omega_{ba}+\mathrm{i}\eta)}\right.$$
$$\left.\left.+\frac{P(c)}{(\omega_3-\omega_{bc}+\mathrm{i}\eta)(\omega_2-\omega_{bc}-\mathrm{i}\eta)(\omega_2-\omega_1-\omega_{ac}-\mathrm{i}\eta)}\right)\right] \quad (59)$$

where we have further made use of Equation (49) to rearrange some frequency combinations. $P(a)$ is the equilibrium probability to be in state a.

These results will be used in the next section to recast the signal in terms of transition amplitudes revealing the underlying molecular processes.

8. CARS SIGNALS RECAST IN TERMS OF TRANSITION AMPLITUDES

We now dissect the CARS signal (59) into components corresponding to various molecular processes. Equation (59) has two contributions, one proportional to $P(a)$, and the other to $P(c)$. For clarity, we only consider the $\sim P(a)$ contribution in detail, and then point out how to do the same for the $\sim P(c)$ part.

The $\sim P(a)$ contribution to Equation (59) exhibits a different structure than the pump–probe signal. This stems from parametric processes. We now demonstrate how to separate these from the contribution of the resonant processes (which assume the generalized Kramers–Heisenberg form).

The $\sim P(a)$ contribution is proportional to (the imaginary part of) $T^{(4)}_{aa}(-\omega_4, \omega_3, -\omega_2, \omega_1) = \mathcal{E}_1\mathcal{E}^*_2\mathcal{E}_3\mathcal{E}^*_4\tilde{T}^{(4)}_{aa}(-\omega_4, \omega_3, -\omega_2, \omega_1)$, corresponding to a fourth-order process leaving the molecule in its initial state. The model of Figure 12, allows for yet another fourth-order process with the order of interactions reversed. The contribution of said process would be proportional to $T^{(4)}_{aa}(-\omega_1, \omega_2, -\omega_3, \omega_4) = \mathcal{E}^*_1\mathcal{E}_2\mathcal{E}^*_3\mathcal{E}_4\tilde{T}^{(4)}_{aa}(-\omega_1, \omega_2, -\omega_3, \omega_4)$. Both processes are depicted diagrammatically in Figure 14.

While according to Equation (59), the signal is proportional to the contribution from the first process, it is clear that both processes

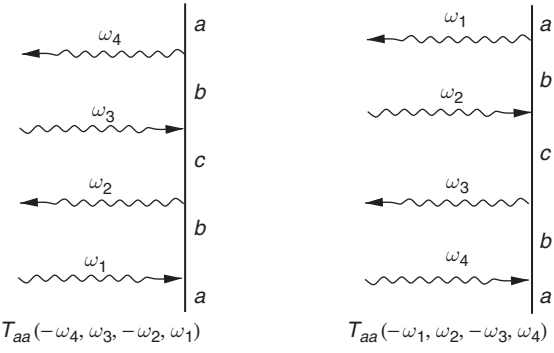

Figure 14 The two fourth-order sequences of interactions contributing to the CARS signal

contribute to the frequency-domain signal. For reasons that will become clear shortly, we rewrite the signal as a sum a symmetric and an asymmetric contribution with respect to the two processes,

$$\mathcal{E}_1\mathcal{E}_2^*\mathcal{E}_3\mathcal{E}_4^*\tilde{T}_{aa}^{(4)}(-\omega_4,\omega_3,-\omega_2,\omega_1) = T_{\mathrm{sym}} + T_{\mathrm{as}}, \tag{60}$$

where

$$\begin{aligned} T_{\mathrm{sym}} \equiv \frac{1}{2}\Big[&\mathcal{E}_1\mathcal{E}_2^*\mathcal{E}_3\mathcal{E}_4^*\tilde{T}_{aa}^{(4)}(-\omega_4,\omega_3,-\omega_2,\omega_1) \\ &+\mathcal{E}_1^*\mathcal{E}_2\mathcal{E}_3^*\mathcal{E}_4\tilde{T}_{aa}^{(4)}(-\omega_1,\omega_2,-\omega_3,\omega_4)\Big] \end{aligned} \tag{61}$$

$$\begin{aligned} T_{\mathrm{as}} \equiv \frac{1}{2}\Big[&\mathcal{E}_1\mathcal{E}_2^*\mathcal{E}_3\mathcal{E}_4^*\tilde{T}_{aa}^{(4)}(-\omega_4,\omega_3,-\omega_2,\omega_1) \\ &-\mathcal{E}_1^*\mathcal{E}_2\mathcal{E}_3^*\mathcal{E}_4\tilde{T}_{aa}^{(4)}(-\omega_1,\omega_2,-\omega_3,\omega_4)\Big] \end{aligned} \tag{62}$$

This is shown diagrammatically in Figure 15. T_{sym} and T_{as} turn out to correspond to resonant and parametric contributions to the signal.

It follows from equation (49) that $\tilde{T}_{aa}^{(4)}(-\omega_4,\omega_3,-\omega_2,\omega_1) = \tilde{T}_{aa}^{(4)}(-\omega_1,\omega_2,-\omega_3,\omega_4)$. This allows us to write T_{as} as

$$T_{\mathrm{as}} = \mathrm{i}\Im(\mathcal{E}_1\mathcal{E}_2^*\mathcal{E}_3\mathcal{E}_4^*)\tilde{T}_{aa}^{(4)}(-\omega_4,\omega_3,-\omega_2,\omega_1), \tag{63}$$

We associate the contribution of the asymmetric part with the parametric process for the following reason. The model allows for two time-reversed fourth-order processes: In one a photon is emitted into mode 4, while in the other a photon is absorbed. The signal is proportional to the difference between the two. Note that these contributions are linear rather than

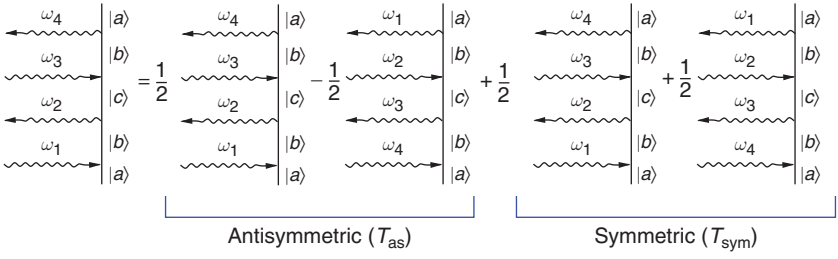

Figure 15 The decomposition of the fourth-order dressed transition amplitude into its symmetric and antisymmetric parts. Time runs from bottom to top. The $\sim P(a)$ part of the CARS signal [Equation (59)] is proportional to the imaginary part of the diagram on the left-hand side

quadratic in the transition amplitudes. The reason is that they come from interference between the fourth-order processes and the zero-order process in which the molecule remains in its initial state.

T_{sym} is the sum of the two possible pathways to make a fourth-order transition starting and ending at a. It can be recast as a contribution from resonant terms using the optical theorem

$$\begin{aligned} 2\Im T_{\mathrm{sym}} = &-\pi\left[\mathcal{E}_1\mathcal{E}_2^*\mathcal{E}_3\mathcal{E}_4^*\tilde{T}^{(1)}_{ba}(\omega_1)\tilde{T}^{(3)*}_{ba}(\omega_2,-\omega_3,\omega_4)+c.c.\right]\delta(\omega_1-\omega_{ba}) \\ &-\pi\left[\mathcal{E}_1\mathcal{E}_2^*\mathcal{E}_3\mathcal{E}_4^*\tilde{T}^{(3)}_{ba}(\omega_3,-\omega_2,\omega_1)\tilde{T}^{(1)*}_{ba}(\omega_4)+c.c.\right]\delta(\omega_4-\omega_{ba}) \\ &-\pi\left[\mathcal{E}_1\mathcal{E}_2^*\mathcal{E}_3\mathcal{E}_4^*\tilde{T}^{(2)}_{ca}(-\omega_2,\omega_1)\tilde{T}^{(2)*}_{ca}(-\omega_3,\omega_4)+c.c.\right]\delta(\omega_1-\omega_2-\omega_{ca}). \end{aligned} \tag{64}$$

For our model this theorem is represented in Figure 16 using the unrestricted loop diagrams.

Having rewritten both T_{as} and T_{sym} in a form with a clear physical interpretation, the $\sim P(a)$ signal can be obtained simply by substituting Equations (63) and (64) in (60), and then (60) in the first term of Equation (59).

To complete the dissection of the signal we need to add the $\sim P(c)$ part. This is not proportional to a single transition amplitude, but it can be brought to this form by first writing $(\omega_3-\omega_{bc}+\mathrm{i}\eta)^{-1}=(\omega_3-\omega_{bc}-\mathrm{i}\eta)^{-1}-2\pi\mathrm{i}\delta(\omega_3-\omega_{bc})$ in Equation (59), and then taking the complex conjugate of the term with three advanced Green's functions. Notably, the resonant term, which has been split off, already has the desired generalized Kramers–Heisenberg form.

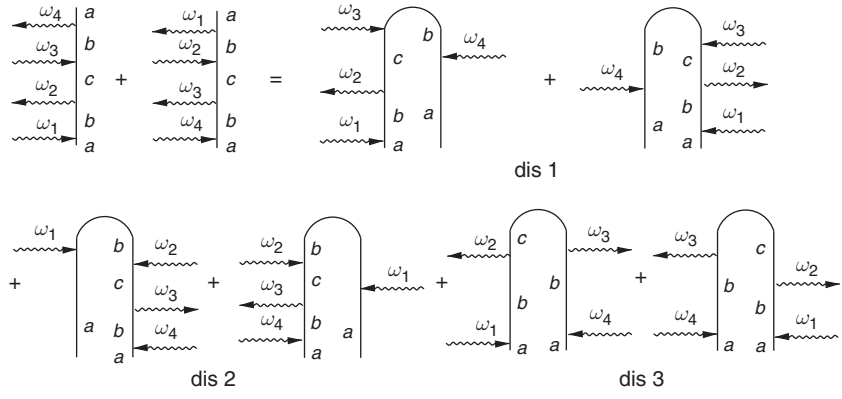

Figure 16 Diagrammatic representation of the optical theorem for our model (64). The six loop diagrams represent the six terms in Equation (64) respectively. Twice the imaginary part of the diagrams on the left is equal to the imaginary part of the diagrams on the right

The non-resonant term can now be dissected following the steps used for the $\sim P(a)$ terms.

Collecting all terms, the signal finally takes the form,

$$S_4 = S_{4,\mathrm{par}} + S_{4,\mathrm{dis}}, \tag{65}$$

with the parametric part

$$S_{4,\mathrm{par}} = \frac{4\pi}{\hbar^4}\delta(\omega_1 - \omega_2 + \omega_3 - \omega_4)\Im(\mathcal{E}_1\mathcal{E}_2^*\mathcal{E}_3\mathcal{E}_4^*)[P(a)\Re\tilde{T}^{(4)}_{aa}(-\omega_4, \omega_3, -\omega_2, \omega_1)$$

$$+P(c)\Re\tilde{T}^{(4)}_{cc}(-\omega_2, \omega_1, -\omega_4, \omega_3)], \tag{66}$$

and the dissipative part

$$\begin{aligned}
S_{4,\mathrm{dis}} = &-\frac{2\pi^2}{\hbar^4}\delta(\omega_1 - \omega_2 + \omega_3 - \omega_4)\\
&\times\Big\{P(a)\Big[\mathcal{E}_1^*\mathcal{E}_2\mathcal{E}_3^*\mathcal{E}_4\tilde{T}^{(3)}_{ba}(\omega_2, -\omega_3, \omega_4)\tilde{T}^{(1)*}_{ba}(\omega_1) + c.c.\Big]\\
&\times\delta(\omega_1 - \omega_{ba}) + P(a)\Big[\mathcal{E}_1\mathcal{E}_2^*\mathcal{E}_3\mathcal{E}_4^*\tilde{T}^{(3)}_{ba}(\omega_3, -\omega_2, \omega_1)\tilde{T}^{(1)*}_{ba}(\omega_4) + c.c.\Big]\\
&\times\delta(\omega_4 - \omega_{ba}) + P(a)\Big[\mathcal{E}_1\mathcal{E}_2^*\mathcal{E}_3\mathcal{E}_4^*\tilde{T}^{(2)}_{ca}(-\omega_2, \omega_1)\tilde{T}^{(2)*}_{ca}(-\omega_3, \omega_4) + c.c.\Big]\\
&\times\delta(\omega_1 - \omega_2 - \omega_{ca}) + P(c)\Big[\mathcal{E}_1^*\mathcal{E}_2\mathcal{E}_3^*\mathcal{E}_4\tilde{T}^{(3)}_{bc}(\omega_4, -\omega_1, \omega_2)\tilde{T}^{(1)*}_{ba}(\omega_3) + c.c.\Big]\\
&\times\delta(\omega_3 - \omega_{bc}) - P(c)\Big[\mathcal{E}_1\mathcal{E}_2^*\mathcal{E}_3\mathcal{E}_4^*\tilde{T}^{(3)}_{bc}(\omega_1, -\omega_4, \omega_3)\tilde{T}^{(1)*}_{ba}(\omega_2) + c.c.\Big]\\
&\times\delta(\omega_2 - \omega_{bc}) - P(c)\Big[\mathcal{E}_1^*\mathcal{E}_2\mathcal{E}_3^*\mathcal{E}_4\tilde{T}^{(2)}_{ac}(-\omega_1, \omega_2)\tilde{T}^{(2)*}_{ac}(-\omega_4, \omega_3) + c.c.\Big]\\
&\times\delta(\omega_2 - \omega_1 - \omega_{ac})\Big\}
\end{aligned} \tag{67}$$

The physical interpretation of the resonant terms in Equation (67) is obvious: They all represent interferences of different possible molecular transitions. Note that the overall sign of each term signifies whether the ω_4 photon is emitted or absorbed.

So far, we have focused on one of the possible CARS signals, namely S_4. The other signals can be similarly dissected into their components. Once this is done, we can combine different signals in order to either enhance or suppress specific molecular pathways. As an example, the signal S_1 can be obtained from S_4 by changing the roles of the field modes 1, 2 and 4, 3 respectively. A simple inspection shows that the parametric part changes its sign under this operation, $S_{1,\mathrm{par}} = -S_{4,\mathrm{par}}$. The combination

$$S_1 + S_4 = S_{1,\mathrm{dis}} + S_{4,\mathrm{dis}} \tag{68}$$

is thus purely dissipative. Further discussion can be found in Rahav et al. (2009). This result will be generalized to arbitrary nonlinear processes in section 10.

9. CARS RESONANCES CAN BE VIEWED AS A DOUBLE-SLIT INTERFERENCE OF TWO TWO-PHOTON PATHWAYS

In the previous section we had dissected the CARS signal into parametric and resonant processes. We now show that the resonant part of the signal originates from an interference of two transition pathways.

We assume that the molecule is initially in its ground state a, and that all frequencies are tuned off electronic resonances so that only Raman resonances are possible. The leading order of the transition amplitude can be found from Equations (25), (28), and (32),

$$P_{a\to c} = \frac{1}{4\pi^2\hbar^4}|\mu_{cb}|^2|\mu_{ba}|^2\left|\int \mathrm{d}\omega \frac{E(\omega)E(\omega_{ca}-\omega)}{\omega-\omega_{ba}+\mathrm{i}\eta}\right|^2. \tag{69}$$

In stimulated CARS the field is made of four narrow-band pulses, centered around frequencies ω_i, $i=1, 2, 3, 4$,

$$E(\omega) = 2\pi\sum_{i=1}^{4}[\mathcal{E}_i\delta_\Delta(\omega-\omega_i) + \mathcal{E}_i^*\delta_\Delta(\omega+\omega_i)]. \tag{70}$$

δ_Δ is a slightly broadened delta function, of width Δ, describing the (normalized) narrowband shape of the pulses.

By substituting Equation (70) and using the dipole transitions of Figure 12 we find that the integral has only two contributions coming from $\omega \simeq \omega_1, \omega_4$.

$$\begin{aligned} P_{a\to c} \simeq \frac{4\pi^2}{\hbar^4}|\mu_{cb}|^2|\mu_{ba}|^2\Bigg|&\frac{\mathcal{E}_1\mathcal{E}_2^*}{\omega_1-\omega_{ba}+\mathrm{i}\eta}\delta_{\Delta'}(\omega_1-\omega_2-\omega_{ca}) \\ &+\frac{\mathcal{E}_4\mathcal{E}_3^*}{\omega_4-\omega_{ba}+\mathrm{i}\eta}\delta_{\Delta'}(\omega_4-\omega_3-\omega_{ca})\Bigg|^2 \end{aligned} \tag{71}$$

The functions $\delta_{\Delta'}$ in Equation (71) result from an integrated product of two of the band shapes δ_Δ. While the width and shape of the $\delta_{\Delta'}$ in Equation (71) are different from those appearing in Equation (70), these are still narrow δ-like shapes.

Equation (71) has a typical form of a double-slit measurement: Two interfering pathways contribute to the resonant Stokes Raman $a\to c$ amplitude. By opening the brackets we find

$$
\begin{aligned}
P_{a\to c} = P^{12}_{a\to c} + P^{34}_{a\to c} + P^{1234}_{a\to c} \simeq \frac{4\pi^2}{\hbar^4}|\mu_{cb}|^2|\mu_{ba}|^2 \\
\times\left(\left|\frac{\mathcal{E}_1\mathcal{E}_2^*}{\omega_1-\omega_{ba}+\mathrm{i}\eta}\right|^2 \delta^2_{\Delta'}(\omega_1-\omega_2-\omega_{ca})\right. \\
+\left|\frac{\mathcal{E}_4\mathcal{E}_3^*}{\omega_4-\omega_{ba}+\mathrm{i}\eta}\right|^2 \delta^2_{\Delta'}(\omega_4-\omega_3-\omega_{ca}) \\
+2\Re\left[\frac{\mathcal{E}_1\mathcal{E}_2^*\mathcal{E}_3\mathcal{E}_4^*}{(\omega_1-\omega_{ba}+\mathrm{i}\eta)(\omega_4-\omega_{ba}-\mathrm{i}\eta)}\right] \\
\left.\times\delta_{\Delta'}(\omega_1-\omega_2-\omega_{ca})\delta_{\Delta'}(\omega_4-\omega_3-\omega_{ca})\right).
\end{aligned}
\tag{72}
$$

Here $P^{12}_{a\to c}(P^{34}_{a\to c})$ represents a pump–probe process involving modes 1 and 2 (3 and 4)[2]. $P^{1234}_{a\to c}$ describes the interference of these two pump–probe pathways.

The double-slit picture has long been established for two-photon absorption and photo electron detection (Glauber, 2007). Equation (72) extends it to Raman processes. The resonant component of the stimulated CARS signal is given by $P^{1234}_{a\to c}$.

For $P(c)=0$ and when all frequencies are tuned off electronic resonances, only one contribution remains in Equation (67). Furthermore, comparison of Equations (67) and (72) gives

$$
S_{4,\mathrm{dis}} = -\frac{1}{2}P^{1234}_{a\to c}. \tag{73}
$$

Equation (73) relates the rate of resonant $a\to c$ transitions to the resonant part of the CARS signal. The $-1/2$ factor can be easily rationalized: The sign comes from the fact that an ω_4 photon is absorbed, while the factor of a $1/2$ signifies that only one of the interfering processes affects the number of photons in mode 4. It is amusing to note that the two processes contributing to the resonant coherent *anti-Stokes* Raman spectroscopy (CARS) signal are in fact $a\to c$ *Stokes* processes!

[2]One may be worried by the appearance of the factor of $\delta^2_{\Delta'}$ in those terms as the limit of narrowband shape is taken, but this is just an artifact resulting from the fact that these pump–probe processes are naturally described in terms of the *rate* of transitions while here we are studying the overall probability. Indeed, $\delta^2_{\Delta'}(x)\sim\delta_{\Delta'}(x)/\Delta'$ and $1/\Delta'$ is proportional to the overall time where the pulses are turned on.

10. PURELY-DISSIPATIVE SPECTROSCOPIC SIGNALS

At the end of Section 8 we had pointed out that it is possible to identify a linear combination of signals such that the parametric contribution is canceled out. The purely dissipative signals, which were defined in section 3.1, accomplish that goal. These signals are obtained by calculating the exchange of energy between the field and the material.

Purely dissipative signals are generally given by Equation (37), which includes contributions from all possible material transitions. Such signals would be useful for spectroscopic applications once some pulse parameters are scanned. This can be done using pulse shaping techniques (Shim & Zanni, 2009; Tian et al., 2003; Weiner, 2009). We represent the field as $\mathcal{E}(\omega) = A(\omega)\mathrm{e}^{\mathrm{i}\phi(\omega)}$, where A is the amplitude of the field while ϕ denotes its phase. Both functions are real. Different transitions may be separated by comparing the response of D to variation of $A(\omega)$ at different frequencies.

We first consider the linear siganl

$$D \simeq \hbar^{-1} \int \mathrm{d}\omega \sum_b \omega |\mu_{ba}|^2 A^2(\omega)\delta(\omega - \omega_{ba}). \tag{74}$$

Variation of the field amplitude gives

$$\sigma(\omega) = \frac{\delta D}{\delta A^2(\omega)} = \sum_b \omega_{ba}|\mu_{ba}|^2 \delta(\omega - \omega_{ba}), \tag{75}$$

which is the linear absorption.

We now turn to Raman processes. We assume that the field is tuned off electronic resonances. The dissipative signal is then

$$D_{\mathrm{CARS}} = \frac{1}{4\pi^2\hbar^3} \sum_c \omega_{ca}|\mu_{cb}|^2|\mu_{ba}|^2 \left| \int \mathrm{d}\omega \frac{\mathcal{E}(\omega)\mathcal{E}(\omega_{ca} - \omega)}{\omega - \omega_{ba} + i\eta} \right|^2. \tag{76}$$

(The optical pulse band shape covers the frequency regime $|\omega| >> \omega_{ca}$, since ω_{ca} is a vibrational transition frequency.)

Raman resonances may be obtained by taking a second-order variation $\delta^2 D/\delta A(\omega_1)\delta A(\omega_2)$. However, these lie on the top of a smooth background resulting from the term where each of the integrals in Equation (76) is varied once. A different approach, which only

requires one variation is to consider a combination of a narrow band and a broad band pulse

$$\mathcal{E}(\omega) \simeq 2\pi\mathcal{E}_0\delta(\omega-\omega_0) + 2\pi\mathcal{E}_0^*\delta(\omega+\omega_0) + \tilde{\mathcal{E}}(\omega). \tag{77}$$

Below we show that variation of the $\sim\mathcal{E}_0^2$ part of D at frequencies near (but different from) ω_0 allows to separate out the different Raman resonances.

The integral in Equation (76) in the RWA can now be approximated by

$$\begin{aligned}\int \mathrm{d}\omega \frac{\mathcal{E}(\omega)\mathcal{E}(\omega_{ca}-\omega)}{\omega-\omega_{ba}+\mathrm{i}\eta} \simeq\ & 2\pi\mathcal{E}_0\mathcal{E}(\omega_{ca}-\omega_0)\frac{1}{\omega_0-\omega_{ba}+\mathrm{i}\eta} \\ & +2\pi\mathcal{E}_0^*\mathcal{E}(\omega_{ca}+\omega_0)\frac{1}{\omega_0-\omega_{bc}+\mathrm{i}\eta},\end{aligned} \tag{78}$$

Variation with respect to the amplitude of the broadband pulse, $A(\omega)$, gives

$$\begin{aligned}\frac{\delta D_{\mathrm{CARS}}}{\delta A(\omega)} \simeq\ & \frac{1}{\pi\hbar^3}\omega_{ca}|\mu_{cb}|^2|\mu_{ba}|^2\Re\left\{\left(\frac{\mathcal{E}_0^*\mathcal{E}(\omega_0-\omega_{ca})}{\omega_0-\omega_{ba}-\mathrm{i}\eta}+\frac{\mathcal{E}_0\mathcal{E}^*(\omega_0+\omega_{ca})}{\omega_0-\omega_{bc}-\mathrm{i}\eta}\right)\right. \\ & \times\left(\frac{\mathcal{E}_0\mathrm{e}^{-\mathrm{i}\phi(\omega_0-\omega_{ca})}}{\omega_0-\omega_{ba}+\mathrm{i}\eta}\left[\delta(\omega-\omega_0+\omega_{ca})+\delta(\omega+\omega_0-\omega_{ca})\right]\right. \\ & \left.\left.+\frac{\mathcal{E}_0^*\mathrm{e}^{\mathrm{i}\phi(\omega_0+\omega_{ca})}}{\omega_0-\omega_{bc}+\mathrm{i}\eta}\left[\delta(\omega-\omega_0-\omega_{ca})+\delta(\omega+\omega_0+\omega_{ca})\right]\right)\right\}.\end{aligned} \tag{79}$$

Equation (79) shows sharp Raman peaks at $\pm\omega_0$ $\pm\omega_{ca}$.

The above considerations illustrate that the variations of dissipative signals with incoming pulse parameters allow to distinguish different material processes. Spectroscopy with dissipative signals should be very convenient. Dissipative signals eliminate the parametric background but are not background-free since the signal is a difference of two large quantities (transmitted minus incoming field intensity).

Chirped pulses (Malinovshy, 2009; Onorato et al., 2007; Pergoraro et al., 2009) as well as coherently shaped pulses in a collinear geometry (Caster et al., 2009; Li et al., 2008; Müller et al., 2009; Ogilvie et al., 2006; Roy et al., 2009; Silberberg, 2009; von Vacano and Motzkus, 2008) were found to be effective in suppressing the parametric signal. The dissipative signals, which can be easily implemented in a collinear geometry and make use of pulse shaping, present a different solution to the same problem.

11. SUMMARY

In this review we have demonstrated that by examining the optical processes from the viewpoint of the matter we can recast the signals in terms of transition amplitudes which represent the molecular wave function and gain new insights. These ideas were demonstrated for two examples: pump-probe (Sections 5 and 6) and CARS (Sections 7 and 8) signals. However, the methods used here are quite general, and apply to other optical measurements, as explained in the following.

Resonant and parametric processes can be clearly separated by recasting the signal in terms of the transition amplitudes. The former take a generalized Kramers–Heisenberg form, namely a product of complex conjugated transition amplitudes, times a resonant δ-function. When considering the rate of transitions between states of matter, one expects to find the amplitudes appearing as complete squares, such as in Equation (71), or sums over complete squares. However, the translation to contributions for optical signals breaks this form. Some of the terms may be omitted since they are not part of the signal under consideration, such as the first two terms in Equation (72), when considering the CARS signal. The terms which are kept should be weighted according to the overall change in the number of photons in the measured mode according to both the ket and the bra. All of these considerations are highly intuitive and easy to follow, but imply that optical signals are not in general of a form of a modulus square of an amplitude.

Parametric processes are linear in the transition amplitude, due to an interference between a high-order process and the zero-order process where the material does not interact with the field. For each n'th order process starting and ending at the same state there is also a time reversed process, where the transitions are "traversed backward." The parametric contribution is proportional to the difference between the direct and time-reversed processes, since a photon which is absorbed in one will be emitted in the other. Such processes were studied in Section 8 for the CARS signal but similar consideration should apply to any type of parametric process.

The contributions of material processes to the optical signal can be understood by recasting it as a sum over terms which correspond to either resonant transitions or parametric processes. We argue that this may be done quite generally, using the following prescription: any loop diagram representing a signal would have retarded Green's functions along the left branch and the advanced ones along the right branch, including the top of the loop. (See rules FD5 and FD7.) One can replace the loop diagram with a different one, where the interactions are shifted along the loop (keeping their relative ordering). This is done either by replacing the last retarded Green's function by an advanced one, or by replacing the first advanced Green's function by a retarded one. This

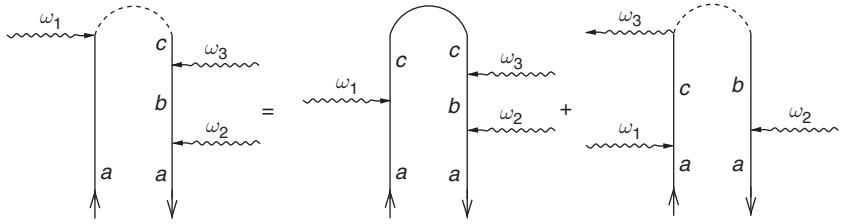

Figure 17 Moving interactions along the loop by adding Kramers–Heisenberg terms. The diagrams are obtained from Figure 8 by (i) moving the second diagram from the right-hand side to the left hand side, and (ii) moving the last interaction from the right branch to the left branch. The second step must be compensated by a sign change due to rule FD9

replacement (Figure 17) must be compensated by an additional term, which is given by an unrestricted loop and has the generalized Kramers–Heisenberg form. Using this operation, any restricted loop diagram can be written as a linear combination of unrestricted ones plus a diagram where all the interactions are on the ket. The diagrams with interactions on the ket should then be divided into symmetric and antisymmetric parts, as was done in Figure 15. The antisymmetric parts are identified with various parametric contributions. The symmetric part can be rewritten as resonant terms using an optical theorem analogous to Equation (64). This last step is non-trivial, and needs to be studied further.

Dissecting nonlinear optical signals into a sum of contributions from resonant and parametric processes enhances our understanding of optical signals and reveals which material processes contribute to each optical signal. In addition, it allows to identify combinations of signals where some material pathways are canceled out and others are enhanced, thus helping the design of new types of measurements.

ACKNOWLEDGMENTS

The support of the National Science Foundation (Grant No. CHE-0745892) and the Chemical Sciences, Geosciences and Biosciences Division, Office of Basic Energy Sciences, Office of Science, U.S. Department of Energy, is gratefully acknowledged.

REFERENCES

Alfano, R. R., & Shapiro, S. L. (1971). Picosecond spectroscopy using the inverse Raman effect. *Chemical Physics Letters*, *8*, 631–633.

Begley, R. F., Harvey, A. B., & Byer, R. L. (1974). Coherent anti-Stokes Raman spectroscopy. *Applied Physics Letters*, *25*, 387–390.

Caster, A. G., Kowarik, S., Schwartzberg, A. M., Nicolet, O., Lim, S.-H., & Leone, S. R. (2009). Observing hydrogen silsesquioxane cross-linking with broadband CARS *Journal of Raman Spectroscopy*, *40*, 770–774.

Cohen, A. E., & Mukamel, S. (2003). Resonant enhancement and dissipation in nonequilibrium van der Waals forces. *Physical Review Letters*, *91*, 233202.

Cohen-Tannoudji, C., Dupont-Roc, J., & Grynberg, G. (1997). *Photons and atoms*. New York: John Wiley & Sons.

Dubetsky, B., & Berman, P. R. (1993). Theory of four-wave mixing using an amplitude approach. *Physical Review A*, *47*, 1294–1313.

Evans, C. L., & Xie, X. S. (2008). Coherent anti-stokes Raman Scattering microscopy: Chemical imaging for biology and medicine. *Annual Review of Analytical Chemistry*, *1*, 883–909.

Glauber, R. J. (2007). *Quantum theory of optical coherence*. Berlin: Wiley-VCH Verlag.

Haché, A., Kostoulas, Y., Atanasov, R., Hughes, J. L. P., Sipe, J. E., & van Driel, H. M. (1997). Observation of coherently controlled photocurrent in unbiased, bulk GaAs. *Physical Review Letters*, *78*, 306–309.

Harbola, U., & Mukamel, S. (2008). Superoperator nonequilibrium Greens function theory of many-body systems; applications to charge transfer and transport in open junctions. *Physics Reports*, *465*, 191–222.

Jones, W. J., & Stoicheff, B. P. (1964). Inverse Raman spectra: Induced absorption at optical frequencies. *Physical Review Letters*, *13*, 657–659.

Kirkwood, J. C., Ulness, D. J., & Albrecht, A. C. (2000). On the classification of the electric field spectroscopies: Application to Raman Scattering. *Journal of Physical Chemistry A*, *104*, 4167–4173.

Kukura, P., McCamant, D. W., & Mathies, R. A. (2007). Femtosecond stimulated Raman spectroscopy. *Annual Review of Physical Chemistry*, *58*, 461–488.

Laimgruber, S., Schachenmayr, H., Schmidt, B., Zinth, W., & Gilch, P. (2006). A femtosecond stimulated raman spectrograph for the near ultraviolet. *Applied Physics B: Lasers Optics*, *85*, 557–564.

Lakshmanna, A., Mallick, B., & Umapathy, S. (2009). Ultrafast Raman loss spectroscopy: A new approach to vibrational structure determination. *Current Science*, *97*, 210–216.

Li, H., Harris, D. A., Xu, B., Wrzesinski, P. J., Lozovoy, V. V., & Dantus, M. (2008). Coherent mode-selective Raman excitation towards standoff detection. *Optical Express*, *16*, 5499–5504.

Lotem, H., Lynch Jr, R. T., & Bloembergen, N. (1976). Interference between Raman resonances in four-wave difference mixing. *Physical Review A*, *14*, 1748–1755.

Malinovsky, V. S. (2009). Optimizing CARS signal using coherent control methods. *Proceedings of SPIE – International Society Optical Engineering*, *7183*, 71830Q.

Mallick, B., Lakshmanna, A., Radhalakshmi, V., & Umapathy, S. (2008). Design and development of stimulated Raman spectroscopy apparatus using a femtosecond laser system. *Current Science*, *95*, 1551–1559.

Marx, C. A., Harbola, U., & Mukamel, S. (2008). Nonlinear optical spectroscopy of single, few, and many molecules: Nonequilibrium Greens function QED approach. *Physical Review* A, *77*, 022110.

Min, W., Lu, S., Chong, S., Roy, R., Holtom, G. R., & Xie, X. S., (2009). Imaging chromophores with undetectable fluorescence by stimulated emission microscopy. *Nature*, *461*, 1105–1109.

Mukamel, S., (1995). *Principles of nonlinear optical spectroscopy*. Oxford: Oxford University Press.

Mukamel, S. (2003). Superoperator representation of nonlinear response: Unifying quantum field and mode coupling theories. *Physical Review E*, *68*, 021111.

Mukamel, S. (2008). Partially-time-ordered Schwinger-Keldysh loop expansion of coherent nonlinear optical susceptibilities. *Physical Review A*, *77*, 023801.

Mukamel, S. (2009). Controlling multidimensional off-resonant-Raman and infrared vibrational spectroscopy by finite pulse band shapes. *Journal of Chemical Physics*, *130*, 054110.

Müller, C., Buckup, T., von Vacano, B., & Motzkus, M. (2009). Heterodyne single-beam CARS microscopy. *Journal of Raman Spectroscopy*, *40*, 809–816.

Nan, X., Tonary, A. M., Stolow, A., Xie, X. S., & Pezacki, J. P. (2006). Intracellular imaging of HCV RNA and cellular lipids by using simultaneous two-photon

fluorescence and coherent anti-stokes Raman scattering microscopies. *Chem Bio Chem*, *7*, 1895–1897.
Newton, R. G. (1982). *Scattering theory of waves and particles*. New York: Springer-Verlag.
Ogilvie, J. P., Beaurepaire, E., Alexandrou, A., & Joffre, M. (2006). Fourier-transform coherent anti-stokes Raman scattering microscopy. *Optics Letters*, *31*, 480–482.
Onorato, R. M., Muraki, N., Knutsen, K. P., & Saykally, R. J. (2007). Chirped coherent anti-Stokes Raman scattering as a high-spectral- and spatial-resolution microscopy. *Optics Letters*, *32*, 2858–2860.
Oron, D., Dudovich, N., Yelin, D., & Silberberg, Y. (2002). Narrow-band coherent anti-stokes Raman signals from broad-band pulse. *Physical Review Letters*, *88*, 063004.
Pegoraro, A. F., Ridsdale, A., Moffatt, D. J., Jia, Y., Pezacki, J. P., & Stolow, A. (2009). Optimally chirped multimodal CARS microscopy based on a single Ti:sapphire oscillator. *Optical Exprers*, *17*, 2984–2996.
Penzkofer, A., Laubereau, A., & Kaiser, W., (1979). High intensity Raman interactions. *Progress in Quantum Electronics, 6* 55–140.
Pestov, D., Murawski, R. K., Ariunbold, G. O., Wang, X., Zhi, M., Sokolov, A. V., et al. (2007). Optimizing the laser-pulse configuration for coherent Raman spectroscopy. *Science*, *316*, 265–268.
Pestov, D., Wang, X., Ariunbold, G. O., Murawski, R. K., Sautenkov, V. A., Dogariu, A., et al. (2008). Single-shot detection of bacterial endospores via coherent Raman spectroscopy. *Proceedings of the National Academy of Sciences of the United States of America*, *105*, 422–427.
Potma E. O., & Xie, X. S. (2008). Coherent anti-stokes raman scattering (CARS) microscopy: Instrumentation and applications. In B. R. Masters & P. T. C. So (Eds.), *Handbook of biomedical nonlinear optical microscopy* (pp. 164–186). New York: Oxford University Press.
Potma, E. O., Evans, C. L., & Xie, X. S. (2006). Heterodyne coherent anti-stokes Raman scattering (CARS) imaging. *Optics Letters*, *31*, 241–243.
Rahav, S., Roslyak, O., & Mukamel, S. (2009). Manipulating stimulated coherent anti-Stokes Raman spectroscopy signals by broad-band and narrow-band pulses. *Journal of Chemical Physics*, *131*, 194510.
Rahav, S., & Mukamel, S. (2010). Stimulated coherent anti-Stokes Raman spectroscopy (CARS) resonances originate from double-slit interference of two-photon Stokes pathways. *Proceedings of the National Academy of Science of United States of America*, *107*, 4825–4829.
Roslyak, O., Marx, C. A., & Mukamel, S. (2009). Generalized Kramers-Heisenberg expressions for stimulated Raman scattering and two-photon absorption. *Physical Review A*, *79*, 063827.
Roy, S., Wrzesinski, P., Pestov, D., Gunaratne, T., Dantus, M., & Gord, J. R. (2009). Single-beam coherent anti-stokes Raman scattering spectroscopy of N_2 using a shaped 7 fs laser pulse. *Applied Physics Letters*, *95*, 074102.
Scully, M. O., & Zubairy, M. S. (1997). *Quantum optics*. Cambridge: Cambridge University Press.
Shen, Y. R. (2002). *The principles of nonlinear optics*. New York: Wiley.
Shim, S. H., & Zanni, M. T. (2009). How to turn your pumpprobe instrument into a multidimensional spectrometer: 2D IR and Vis spectroscopies via pulse shaping. *Physical Chemistry Chemical Physics*, *11*, 748–761.
Silberberg, Y. (2009). Quantum coherent control for nonlinear spectroscopy and microscopy. *Annual Review of Physical Chemistry*, *60*, 277–292.
Tian, P., Keusters, D., Suzaki, Y., & Warren, W. S. (2003). Femtosecond phase-coherent two-dimensional spectroscopy. *Science*, *300*, 1553–1555.
von Vacano, B., & Motzkus, M. (2008). Time-resolving molecular vibration for microanalytics: Single laser beam nonlinear Raman spectroscopy in simulation and experiment. *Physical Chemistry Chemical Physics*, *10*, 681–691.
Weiner, A. M. (2009). *Ultrafast optics*. Hoboken: John Wiley & Sons.
Wilson, K. C., Lyons, B., Mehlenbacher, R., Sabatini, R., & McCamant, D. W. (2009). Two-dimensional femtosecond stimulated Raman spectroscopy: Observation of cascading Raman signals in acetonitrile. *Journal of Chemical Physics*, *131*, 214502.